

國立臺灣大學工學院化學工程研究所

碩士論文

Graduate Institute of Chemical Engineering

College of Engineering

National Taiwan University

Master Thesis



錐狀奈米孔道內離子種類及聚電解質改質表面

對離子傳輸行為之影響

Ion Transport Properties in Conical Nanopores:  
Effect of type of salts and Polyelectrolyte Brushes  
Functionalized Surface

楊淑端

Shu-Tuan Yang

指導教授：徐治平 博士

Advisor: Jyh-Ping Hsu, Ph.D.

中華民國 106 年 6 月

June 2017

## 誌謝



轉眼間兩年的研究生生活過去了，在這段不長不短的日子裡，特別感謝許多人在研究上的幫助，讓我能完成這篇論文。感謝老師這兩年的指導，也給予我們參加研討會的機會。感謝志原學長從頭教導我們研究的內容，即使很忙也願意回答我們的問題，幫助我許多。

也謝謝 309 實驗室的學長們同學們還有學弟妹們。雖然陳俞閔對電腦的軟硬體都不太熟悉，但之前認真的程度值得學習，也為實驗室帶來許多歡笑。林子暉總會一個人默默做事，即便不是他的事也會去完成，雖然我對統計方面不太熟悉，沒能給你什麼幫助，朱育佑也是，希望你們的研究一切順利。采葳永哲在實驗室也待了很久，跟她也討論了很多研究上的東西，你們都很厲害，相信你們可以完成許多研究。

## 中文摘要



圓錐奈米孔道有不對稱的幾何形狀，加上若孔道開口與電雙層厚度相當時，會引起許多特別的電動力學現象，像是離子電流整流效應(ICR)。首先我們考慮不同電解質溶液 LiCl、NaCl、KCl，並研究電滲透流(EOF)對整流效應的影響。我們發現有無考慮電滲透流對整流效應係數( $R_f$ )的程度有很大的影響。如果沒有考慮電滲透流，LiCl 水溶液在不同外加電壓下的整流效果是三者中最好的。若考慮電滲透流，則不同溶液的整流效果與外加電壓大小相關。

接著，我們討論一合成圓錐狀奈米孔道，其表面塗佈一層 pH 可調節之聚電解質。考慮在外加電場下，溶液酸鹼值 pH、溶液鹽濃度、施加電壓不同對離子傳輸行為及離子選擇性之影響。我們發現溶液導電度會因 pH、溶液鹽濃度不同有很大的影響，而離子選擇性則同時受 pH、溶液鹽濃度及施加電壓的影響。

關鍵字：圓錐狀奈米孔道；離子電流整流效應；電滲透流；離子種類；電荷可調節之聚電解質層；電雙層

## ABSTRACT



The influence of electroosmotic flow (EOF) on the behavior of the ionic current rectification (ICR) in a conical nanopore connecting two large identical reservoirs is investigated. In particular, the effect of the type of salt is examined by considering LiCl, NaCl, and KCl. We show that neglecting EOF is capable of influencing ICR both quantitatively and qualitatively. If EOF is neglected, the rectification factor at each level of the applied electric potential bias across the two reservoirs for the case of LiCl (KCl) is always the largest (smallest). However, if EOF is taken into account, the relative magnitude of the rectification factors for various salts depends upon the level of the applied electric potential bias. This behavior is consistent with the experimental observation in the literature and can be explained by the degree of ion enrichment / depletion in a nanopore.

Furthermore, the behaviors of the nanopore conductance and ion selectivity of a conical nanopore surface modified by a polyelectrolyte (PE) layer are studied by adjusting the pH, the bulk salt concentration, and the level of an applied potential bias, and the underlying mechanisms investigated in detail. We show that the conductance is sensitive to the variation in the solution pH, and the conical nanopore has ion current rectification (ICR) behavior. The ion selectivity of the nanopore is influenced significantly by both the solution pH and the level of the applied potential bias. We

show that the transport behavior of ions can be tuned easily by adjusting the level of pH, salt concentration, and applied potential bias, thereby providing useful information for future designing of conical nanopores.



*Keywords:* conical nanopore; ion current rectification; electroosmotic flow; type of salts; pH-tunable polyelectrolyte brushes; electric double layer

# TABLE OF CONTENTS



中文摘要.....	I
ABSTRACT.....	II
TABLE OF CONTENTS.....	IV
LIST OF FIGURES.....	V
LIST OF TABLES.....	IX
CHAPTER 1: Effect of type of salts .....	1
References.....	14
CHAPTER 2: Effect of polyelectrolyte functionalized surface .....	28
References.....	46
CHAPTER 3: Conclusions.....	63
APPENDIX A.....	65
Reference.....	69

## LIST OF FIGURES



**Figure 1-1.** Schematic of a conical nanopore with  $L_n=1000$  nm,  $R_t=5$  nm,  $R_b=28$  nm, half cone angle  $\theta=1.32^\circ$ ,  $L_r=R_r=800$  nm, and  $\sigma_w=-1$  e/nm<sup>2</sup>. ..... 22

**Figure 1-2.** Current-voltage curves of a conical nanopore for various types of salt with and without considering EOF at  $C_0=50$  mM. Black solid curve: KCl, (PNP+NS) model; open squares: KCl, PNP model. Red dashed curve: NaCl, (PNP+NS) model; open circles: NaCl, PNP model. Blue dotted curve: (PNP+NS) model; open triangles: LiCl, PNP model. .... 23

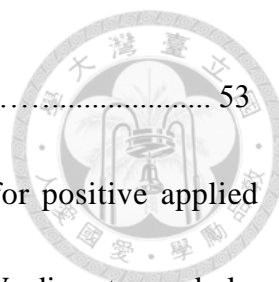
**Figure 1-3.** Variation of the current rectification factor  $R_f$  with applied voltage bias  $V$  for various types of salt at  $C_0=50$  mM. (a) PNP model, (b) (PNP+NS) model. .... 24

**Figure 1-4.** Axial variation in the cross sectional averaged concentrations under various conditions at  $C_0=50$  mM. (a) PNP model at  $V=-0.2$ V, (b) (PNP+NS) model at  $V=-0.2$ V, (c) PNP model at  $V=-2$ V, (d) (PNP+NS) model at  $V=-2$ V. .... 25

**Figure 1-5.** Axial variations in the cross sectional averaged concentration difference at various levels of the applied bias for the present (PNP+NS) model. (a)  $V=-0.2$  V, (b)  $V=-2$  V, (c)  $V=0.2$  V, (d)  $V=2$  V. .... 26

**Figure 1-6.** Variation of the current rectification factor  $R_f$  with surface charge density  $\sigma_w$  for various types of salt at  $C_0=50$  mM. (a)  $|V|=0.2$  V, (b)  $|V|=2$  V. .... 27

**Figure 2-1.** Schematic representation of the transport of ions in a polyelectrolyte modified



conical nanopore (not to scale) subject to an applied potential bias..... 53

**Figure 2-2.** Variation of the nanopore conductance  $G$  with pH for positive applied potential bias, (a), and negative potential bias, (b). Curves:  $|V|=1$  V; discrete symbols:  $|V|=0.3$  V. Black curves:  $C_b=1$  mM; red curves:  $C_b=100$  mM..... 54

**Figure 2-3.** Variation of the volume averaged charge density of the PE layer  $\rho_a^*$  with pH for positive, (a), and negative, (b), applied potential bias. Curves:  $|V|=1$  V; discrete symbols:  $|V|=0.3$  V. Black curves:  $C_b=1$  mM; red curves:  $C_b=100$  mM..... 55

**Figure 2-4.** Axial variation in the cross-sectional averaged ionic concentrations  $C_{a,j}$  at pH 3 for  $C_b=1$  mM, (a) and (b), and  $C_b=100$  mM, (c) and (d). Black curves:  $|V|=0.3$  V; red curves:  $|V|=1$  V. Solid curves: total cation concentration ( $C_1+C_3$ ); dash-dotted curves: total anion concentration ( $C_2+C_4$ ). (a) and (c):  $V>0$ ; (b) and (d):  $V<0$ ..... 56

**Figure 2-5.** Axial variation in the cross-sectional averaged ionic concentrations  $C_{a,i}$  at pH 6 for  $C_b=1$  mM, (a) and (b), and  $C_b=100$  mM, (c) and (d). Black curves:  $|V|=0.3$  V; red curves:  $|V|=1$  V. Solid curves: total cation concentration ( $C_1+C_3$ ); dash-dotted curves: total anion concentration ( $C_2+C_4$ ). (a) and (c):  $V>0$ ; (b) and (d):  $V<0$ . ..... 57

**Figure 2-6.** Axial variation in the cross-sectional averaged ionic concentrations  $C_{a,i}$  at pH 9 for  $C_b=1$  mM, (a) and (b), and  $C_b=100$  mM, (c) and (d). Black curves:  $|V|=0.3$  V; red curves:  $|V|=1$  V. Solid curves: total cation concentration ( $C_1+C_3$ ); dash-dotted curves: total anion concentration ( $C_2+C_4$ ). (a) and (c):  $V>0$ ; (b) and (d):  $V<0$ . ..... 58



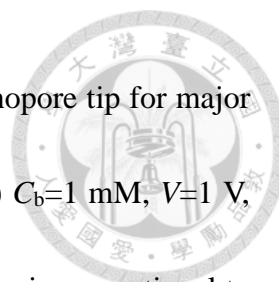


**Figure 2-7.** The fluid velocity and concentration profile near the nanopore tip for major ions. (a) and (b):  $C_1$ ; (c):  $C_2$ . (a)  $C_b=100$  mM,  $V=1$  V, and pH 9; (b)  $C_b=1$  mM,  $V=1$  V, and pH 9; (c)  $C_b=1$  mM,  $V=-1$  V, and pH 2.2. The magnitude of arrow is proportional to fluid velocity. .... 59

**Figure 2-8.** Variation of the nanopore selectivity  $S$  with pH for positive, (a), and negative, (b), potential bias. Curves:  $|V|=1$  V; discrete symbols:  $|V|=0.3$  V. Black curves:  $C_b=1$  mM; red curves:  $C_b=100$  mM. .... 60

**Figure 2-9.** Variation of the cross-sectional averaged ion flux of species  $i$  at  $z=0$  with pH for  $V=+1$  V, (a) and (c), and  $V=-1$  V, (b) and (d). (a) and (b):  $C_b=1$  mM; (c) and (d):  $C_b=100$  mM. Black solid, red dash-dotted, blue dotted, and blue dotted curves are for  $K^+$ ,  $Cl^-$ ,  $H^+$ , and  $OH^-$ , respectively. .... 61

**Figure S1.** Variation of ionic current with applied electric potential bias. Solid curve: experimental data of Liu *et al.*<sup>1</sup>; discrete symbols: values predicted by the present model for various values of  $\sigma_w$  at  $L_n=10000$  nm,  $R_t=26$  nm,  $R_b=2000$  nm, and  $C_0=50$  mM. .... 65

**Figure S2.** The fluid velocity and concentration profile near nanopore tip at  $V=-0.5V$ , (a), and  $V=-1.5V$ , (b). The arrow scale is proportional to fluid velocity. .... 66

**Figure S3.** Axial variation in the cross sectional averaged concentrations under various conditions at  $C_0=50$  mM. (a) PNP model at  $V=0.2V$ , (b) (PNP+NS) model at  $V=0.2V$ , (c)

PNP model at  $V=2V$ , (d) (PNP+NS) model at  $V=2V$ . ..... 67

**Figure S4.** Axial variations in the cross sectional averaged concentration difference for various levels of applied bias; PNP model is applied. (a)  $V=-0.2 V$ , (b)  $V=-2 V$ , (c)  $V=0.2 V$ , (d)  $V=2 V$ . ..... 68

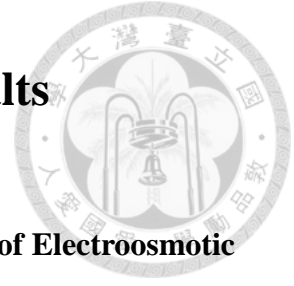


# LIST OF TABLES

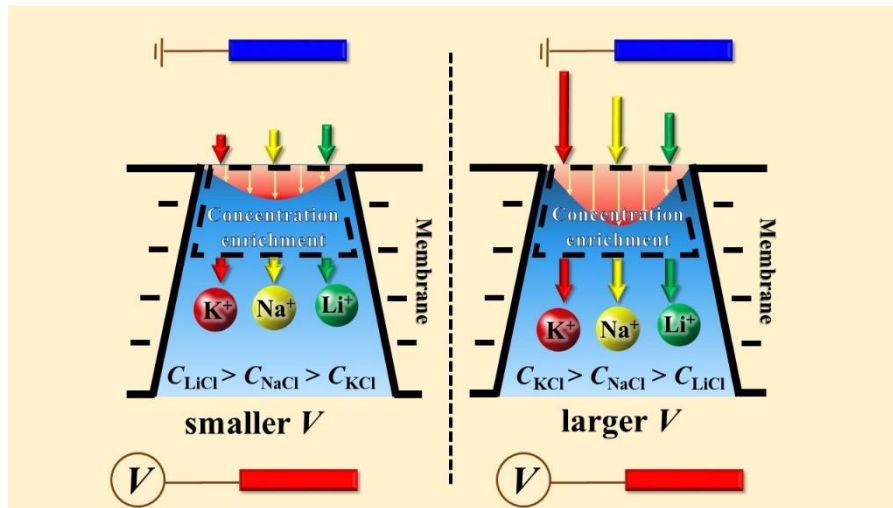


**Table 2-1.** Values of the nanopore conductance  $G$  under various conditions..... 62

# CHAPTER 1: Effect of type of salts



## Ionic Current Rectification in a Conical Nanopore: Influences of Electroosmotic Flow and Type of Salt






## 1-1. Introduction

Due to its potential in simulating biological ion channels and devices in various applications, synthetic nanopores have drawn the attention of researchers of various fields.<sup>1-10</sup> For example, the sequence of DNAs can be determined by measuring the ionic current signals as they translocate through a nanopore.<sup>11-18</sup> A detailed understanding of the electrokinetics and the associated mechanisms for the transport phenomena occur in nanopores is of practical significance.

Ionic current rectification (ICR),<sup>19-22</sup> where the ionic current arising from an applied potential bias exhibits a preferential direction or diode-like behavior, is one of the interesting and important electrokinetics behaviors of nanopores. Several mechanisms have been proposed to explain this phenomenon, including, for example, ion enrichment/depletion,<sup>23-24</sup> influence of nanopore tip,<sup>25-26</sup> and electrokinetic trapping of mobile ions.<sup>27-28</sup> Ion selectivity<sup>29-32</sup> is another specific behavior of conical nanopores. This behavior is significant when the nanopore radius is comparable to Debye length, so that electric double layer (EDL) overlapping is important. In this case, because coions are repelled electrically by the nanopore the measured current is mostly contributed by counterions. Ion selectivity is influenced by factors such as the level of applied potential bias, tip radius, and nanopore length.<sup>25-26, 33-34</sup>

Often, a model comprising Poisson and Nernst-Planck (PNP) equations is adopted to



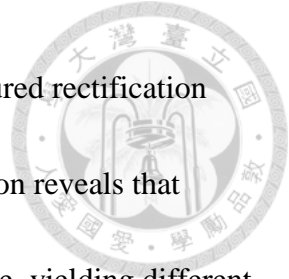
describe the experimentally observed data for many reserches.<sup>25</sup> Since the effect of electroosmotic flow (EOF)<sup>35-36</sup> is neglected in this model, it can be inapplicable under certain circumstances. For instance, in a study of the ion transport in nanofluidic channels, Daiguji *et al.*<sup>37</sup> concluded that the higher the surface charge density of a channel the more important the EOF effect is, and the ion transport inside is influenced appreciably by the channel surface. Assuming constant surface charge density, Ai *et al.*<sup>38</sup> solved a set of Poisson and Nernst-Planck and Navier-Stokes (PNP+NS) equations. They concluded that the EOF effect is significant if the applied voltage is high, and both the surface charge and the thickness of double layer take a medium large value. The analysis of Ai *et al.*<sup>38</sup> was extended to the case of channels having a charge-regulated surface by Lin *et al.*<sup>39</sup> They illustrated that the EOF effect should not be neglected if the bulk salt concentration takes a medium high level and the applied potential bias is high.

Many attempts have been made on examining the influence of the nanopore properties, such as its surface charge and geometry, and solution properties including pH and salt concentration, on the associated ICR behavior. In contrast, that influence of the types of ionic species in the liquid phase receives much less attention. The influence of multivalent cations on the ICR behavior of a biological pore was studied both experimentally<sup>40-43</sup> and theoretically.<sup>44-45</sup> It was found that these cations are capable of inducing a charge inversion on the pore walls.<sup>40</sup> Valisko *et al.*<sup>46</sup> reported that due to the

binding of  $\text{Ca}^{2+}$ , an originally highly negatively charged silica surface might become positively charged, known as overcharging, and anion-selective.



For simplicity, relevant previous studies, both experimental and theoretical, adopted an aqueous KCl solution as the model system because the diffusivity of  $\text{K}^+$  is essentially the same as that of  $\text{Cl}^-$ , so that the electrophoresis effect<sup>47</sup> can be neglected. However, it was reported that the translocation of DNA through a nanopore is influenced by the types of salt solution,<sup>48</sup> and was explained by the interaction of cations with DNA molecules. In an attempt to understand how cations affect the ICR behavior of  $\alpha$ -hemolysin channel, Bhattacharya *et al.*<sup>49</sup> considered various alkali chloride salts. They found that the magnitude of the rectification factors for the cations considered follows the order:  $\text{Li}^+ < \text{Na}^+ < \text{K}^+ < \text{Rb}^+ < \text{Cs}^+$ , and the difference was attributed to the difference in the affinity of cations to the charged residues of the channel. The interaction of cations with the charged channel surface yields a depletion in mobile cations inside the channel. A detailed understanding of the ions-pore surface interaction is helpful for enhancing the detection capability of nanopore sensors. Piguet *et al.*<sup>48</sup> examined the influence of EOF on the electrokinetic flow of aqueous LiCl and KCl solutions in the  $\alpha$ -hemolysin channel. Due to a more significant EOF, LiCl solution shows a larger anion selectivity than KCl. Adopting a PET nanopore, Gamble *et al.*<sup>50</sup> examined the influence of the types of ionic species on its rectification behavior. A molecular dynamics (MD) simulation



was used to explain the difference between the experimentally measured rectification factor and that predicted by a PNP model. The result of MD simulation reveals that different cations have different binding ability to the nanopore surface, yielding different degree of surface charge reduction. Although this is interesting, the ionic current predicted by the MD simulation deviates appreciably from the experiment data, presumably due to the limitation in the simulation scale of the approach adopted.

Adopting a continuum model, the ionic transport in a conical nanopore is analyzed in this study, taking account of the effects of surface charge density and EOF. Three types of typical monovalent aqueous salt solutions are considered: KCl, NaCl, and LiCl.

## 1-2. Theoretical model

We consider a conical nanopore of length  $L_n$ , tip radius  $R_t$ , base radius  $R_b$  connecting two identical large reservoirs of length  $L_r$  and radius  $R_r$ , as shown in Figure 1-1. The system is filled with an incompressible aqueous salt solution. An electric potential bias  $V$  is applied across the two reservoirs with the furthest surface of the tip side reservoir grounded. The wall of the nanopore has a fixed charge density  $\sigma_w$ .

The ions in the system are driven by  $-\nabla\phi$  from one reservoir to the other. At steady state, their transport can be described by the Nernst-Planck equations below:

$$\nabla \cdot \mathbf{N}_j = 0 \quad (1.1)$$





$$\mathbf{N}_j = C_j \mathbf{u} - D_j (\nabla C_j + \frac{F z_j C_j}{RT} \nabla \phi) \quad (1.2)$$

$\mathbf{N}_j$ ,  $C_j$ ,  $D_j$ , and  $z_j$  represent the ionic flux, the concentration, the diffusion coefficient, and the valence of ionic species  $j$ .  $\mathbf{u}$ ,  $F$ ,  $R$ , and  $T$  are the fluid velocity, Faraday constant, gas constant, and the absolute temperature, respectively. The electric potential  $\phi$  in Eq. (1.2)

is described by the following Poisson equation:

$$\nabla^2 \phi = -\frac{\rho_e}{\varepsilon} = -\sum_{j=1}^2 \frac{F z_j C_j}{\varepsilon} \quad (1.3)$$

$\varepsilon$  and  $\rho_e$  are the fluid permittivity and the space charge density, respectively.

Since the fluid flow in the nanopore driven by  $-\nabla \phi$  is in the creeping flow region, the corresponding flow field can be described by the equation of continuity and the Navier-Stokes equation

$$\mu \nabla^2 \mathbf{u} - \nabla p - \rho_e \nabla \phi = \mathbf{0} \quad (1.4)$$

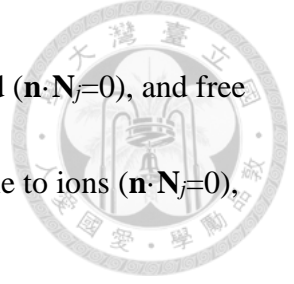
$$\nabla \cdot \mathbf{u} = 0 \quad (1.5)$$

$\mu$  is fluid viscosity, and  $p$  the hydrodynamic pressure.

If we let  $S$  be the surface of the reservoir end, the ionic current  $I$  can be evaluated by

$$I = \int_S F \left( \sum_j z_j \mathbf{N}_j \right) \cdot \mathbf{n} dS \quad (1.6)$$

Suppose that no external pressure gradient is applied across the two reservoirs, and they are large enough so that the salt concentration on the furthest surface of the tip-end reservoir reaches the bulk value ( $C_j=C_0$ ). In addition, the electric potential on that surface vanishes,  $\phi(z=0.5L_n+L_r)=0$ , and that on the furthest surface of the base-end



reservoir  $\phi(z=-0.5L_n-L_r)=V$ . The side boundaries of reservoir are rigid ( $\mathbf{n}\cdot\mathbf{N}_j=0$ ), and free of charge ( $-\mathbf{n}\cdot\nabla\phi=0$ ). The wall of the conical nanopore is impermeable to ions ( $\mathbf{n}\cdot\mathbf{N}_j=0$ ), no slip ( $\mathbf{u}=\mathbf{0}$ ), and has a fix surface charge  $\sigma_w (-\mathbf{n}\cdot(\epsilon\nabla\phi))$ .

Note that if the effect of electroosmotic flow is neglected, Eqs. (1.4) and (1.5) need not be solved, defined as PNP model, for convenience. Otherwise, we have to solve Eqs. (1)-(5), defined as (PNP+NS) model in subsequent discussion.

### 1-3. Results and discussion

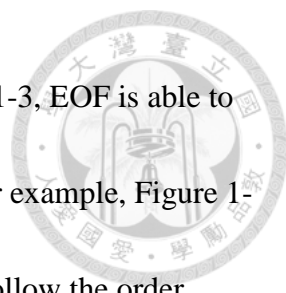
This model is solved numerically by a finite element based commercial software, COMSOL (version 4.3a, <http://www.comsol.com>). The behaviors of the ionic transport in the nanopore under various conditions are examined. The present (PNP+NS) model is first calibrated by fitting it to the experiment data of Liu *et al.*<sup>51</sup> for a conical nanopore and an aqueous KCl solution. The results obtained are shown in Figure S1 of Supporting Information. For illustration, we assume pH=7,  $L_n=1000$  nm,  $R_t=5$  nm,  $R_b=28$  nm,  $L_r=R_r=800$  nm,  $\sigma_w=-1$  e/nm<sup>2</sup> (e.g., a PET nanopore<sup>50, 52</sup>), and  $C_0=50$  mM. The half cone angle  $\theta=1.32^\circ$  is similar with the angle of the nanopore used in the experiment of Gamble *et al.*<sup>50</sup> Three types of salts are considered: KCl, NaCl, and LiCl. Other parameter values adopted are  $F=96500$  C/mol,  $R=8.314$  J/mol K,  $T=298$  K,  $\mu=0.001$  Pa s,  $\epsilon=6.95\times 10^{-10}$  F/m,  $D_{K^+}=1.96\times 10^{-9}$  m<sup>2</sup>/s,  $D_{Na^+}=1.33\times 10^{-9}$  m<sup>2</sup>/s,  $D_{Li^+}=1.03\times 10^{-9}$  m<sup>2</sup>/s,



and  $D_{Cl^-} = 2.03 \times 10^{-9} \text{ m}^2/\text{s}$ .


In subsequent discussion,  $\sigma_w$ ,  $V$ , and the types of cation are examined for their influences on current rectification. Figure 1-2 shows the simulated current-voltage ( $I$ - $V$ ) curves for various types of salt. Both the results for the case where EOF effect is considered and the corresponding results for the case where it is neglected are presented. This figure shows the preferential direction of the ionic current from the nanopore tip to its base, regardless the EOF effect is considered or not. This is because if  $V > 0$  (electric field directs from nanopore base to its tip), the cation-selective nature of the nanopore yields ion depletion inside.<sup>53</sup> In contrast, if  $V < 0$ , both cations and anions are enriched in the nanopore, thereby raising the ionic current. This phenomena is known as ionic current rectification (ICR). For both positive and negative voltage bias, the magnitude of ionic current follows the order  $|I(\text{KCl})| > |I(\text{NaCl})| > |I(\text{LiCl})|$ , which can be explained by the difference in the mobility of the ionic species considered. Figure 1-2 reveals that the presence of EOF has the effect of raising the ionic current, especially when a negative voltage bias is applied. This is because EOF facilitates the ion transport.<sup>38</sup>

To measure the current rectification effect of a nanopore, we define the rectification factor  $R_f = |I(V=v)| / |I(V=-v)|$ .<sup>50</sup> Figure 1-3 summarizes the simulated variation in  $R_f$  with the applied voltage bias  $V$  for various types of salt. Both the results for the case where EOF is neglected (i.e., PNP model), and those for the case where EOF is



considered (i.e., (PNP+NS) model) are presented. As seen in Figure 1-3, EOF is able to influence both quantitatively and qualitatively the behavior of  $R_f$ . For example, Figure 1-3a reveals that if EOF is neglected, the values of  $R_f$  for various salt follow the order  $R_f(\text{LiCl}) > R_f(\text{NaCl}) > R_f(\text{KCl})$ . This behavior is also reported by Gamble *et al.*<sup>50</sup> in their theoretical work, and was explained by the difference in the bulk conductivity. However, as seen in Figure 1-3b, if EOF is taken into account, then for  $V$  lower than ca. 0.9 V,  $R_f(\text{LiCl}) > R_f(\text{NaCl}) > R_f(\text{KCl})$ , but this order is reversed when  $V$  exceeds ca. 0.9 V. This phenomenon is consistent with the experimental observation of Gamble *et al.*,<sup>50</sup> where it was explained by a molecular dynamics (MD) simulation based on a model PET pore. They concluded that the binding abilities of the types of cation examined to the PET membrane surface follow the order:  $\text{Li}^+ > \text{Na}^+ > \text{K}^+$ . Since the higher the binding ability of cations the lower the effective surface charge density of the nanopore, the resultant values of  $R_f$  are different. However, the simulated values of  $R_f$  based on MD deviate appreciably from the experimental data. This might arise from the limitation of MD: the thickness of PET membrane was assumed the value of 10 nm, which is too thin to observe the effect of ion depletion/enrichment.<sup>26</sup>

To explain the influence of EOF on  $R_f$  seen in Figure 1-3b, we examine the ionic distributions in the nanopore. Figure 1-4 reveals that if the applied voltage bias is low ( $V = -0.2\text{V}$ , Figure 1-4a and Figure 1-4b), the ionic distributions for the case where EOF is



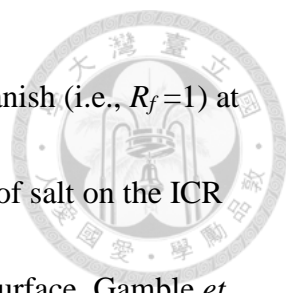
neglected (i.e., PNP model) are similar to those for the case where it is taken into account (i.e., (PNP+NS) model). That is, if the applied voltage bias is low, the EOF effect can be neglected, as observed in several previous works.<sup>38</sup> However, as indicated in Figure 1-4c and Figure 1-4d, if the applied voltage bias is sufficiently high, this effect becomes significant. In this case, the behavior of the ionic distributions based on a PNP model remains about the same as that in Figure 1-4a, but becomes quite different if a (PNP+NS) model is applied. This is because the degree of EOF increases with increasing with applied voltage bias,<sup>38</sup> as illustrated in Figure S2 of Supporting Information. This figure also reveals that, due to EOF effect, the concentration profile is influenced appreciably by the applied voltage bias. In addition, as seen in Figure S3 of Supporting Information, if a positive voltage bias is applied, the ionic distributions for the types of ionic species considered are about the same. This suggests that the ICR behavior of the nanopore for types of salt examined are dominated mainly by the ionic current at negative voltage bias. However, this fails to explain the rectification behavior when the applied voltage bias is sufficiently small since the ionic distributions are almost the same for the types of salt examined for both PNP and (PNP+NS) models, as illustrated in Figure 1-4a, 1-4b, S3a, and S3b.

In the absence of an applied voltage bias ( $V=0$  V), the attraction of counterions (cations) by the charged wall of the nanopore establishes naturally an ion distribution in



its interior. When an applied voltage bias is applied this distribution is influenced, yielding ion enrichment/depletion in the nanopore. To illustrate this, we plot the difference in the ionic distribution,  $\Delta\bar{C}_t = (\bar{C}_1 - \bar{C}_1^0) + (\bar{C}_2 - \bar{C}_2^0)$ , due to the application of the voltage bias in Figure 1-5, where  $\bar{C}_i^0$  denotes the  $\bar{C}_i$  in the nanopore at 0 V. This figure reveals that the degree of ion enrichment/depletion depends upon the types of cation. As seen in Figure 1-5a, if a small negative voltage bias ( $V=-0.2$  V) is applied, an ion enrichment arising from the applied voltage bias occurs, and its degree follows the order  $\text{LiCl} > \text{NaCl} > \text{KCl}$ . However, this order is reversed ( $\text{KCl} > \text{NaCl} > \text{LiCl}$ ) if a large negative voltage bias ( $V=-2$  V) is applied, as shown in Figure 1-5b. This reasonably explains the observed voltage-dependent ICR behaviors of the salts examined. Note that as shown in Figure 1-5c and 1-4d that if a positive voltage bias is applied, the ionic distributions for the types of salt examined are essentially the same. For comparison, the concentration difference  $\Delta\bar{C}_t$  for the corresponding PNP model is also plotted in Figure S4 of Supporting Information, which reveals that the influence of the type of salt is negligible. We conclude that the difference of the ionic distribution in the nanopore among the salts examined mainly arises from the effect of EOF.

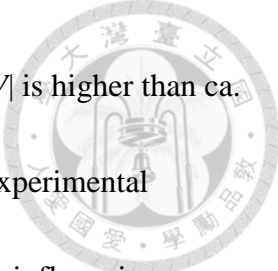
Figure 1-6 reveals that for the types of salt considered, the current rectification factor  $R_f$  exhibits a local maximum as the surface charge density varies. The presence of the local maximum in  $R_f$  for the case of KCl was also observed and thoroughly discussed in



other theoretical studies.<sup>38,54</sup> Note that the rectification effect must vanish (i.e.,  $R_f=1$ ) at zero surface charge.<sup>55</sup> Previous studies for the influence of the types of salt on the ICR behavior of a nanopore focused on the affinity between ions and its surface. Gamble *et al.*<sup>50</sup>, for example, suggested that the difference between the experimentally measured rectification factor and that predicted by a PNP model arises from a reduction in surface charge due to surface binding of ions. Adopting a (PNP+NS) model, we show that the experimentally observed behavior of  $R_f$  can also be explained by the presence of EOF. Figure 1-6a also reveals that at  $|V|=0.2$  V,  $R_f$  follows the order LiCl>NaCl>KCl for the range of the surface charge density examined. However, if  $|V|$  is raised to 2 V, this order is reversed when the surface charge density is sufficiently large, as seen in Figure 1-6b. Again, this suggests that EOF plays a critical role in ion-species rectification.

#### 1-4. Conclusions

The influence of electroosmotic flow (EOF) on the ionic current rectification (ICR) behavior of a conical nanopore is investigated by considering three types of aqueous salt solution, namely, LiCl, NaCl, and KCl. We show that if the EOF effect is neglected, the magnitudes of the rectification factor  $R_f$  of these solutions rank as LiCl>NaCl>KCl at each level of the applied potential bias  $V$ . However, if that effect is considered, the relative magnitudes of the  $R_f$  of the salts examined depend upon the level of  $V$ . If  $|V|$  is




lower than ca. 0.9 V,  $R_f$  follows the order of  $\text{LiCl} > \text{NaCl} > \text{KCl}$ , but if  $|V|$  is higher than ca. 0.9 V, the order becomes  $\text{KCl} > \text{NaCl} > \text{LiCl}$ , which is consistent with experimental observation. At a higher  $V$ , the EOF effect is more significant, thereby influencing more appreciably the ionic concentration inside the nanopore. If  $V < 0$ , the degrees of concentration enrichment for different types of ions differ appreciably. The concentration enrichment of  $\text{LiCl}$  increases most if  $V$  is low, while that of  $\text{KCl}$  increases most if  $V$  is high, yielding the inversion of the order of  $R_f$  mentioned above. We conclude that, in addition to ionic binding, EOF also plays a crucial role in ion-species current rectification, especially when  $V$  is high.







## REFERENCES

1. Sa, N. Y.; Lan, W. J.; Shi, W. Q.; Baker, L. A., Rectification of Ion Current in Nanopipettes by External Substrates. *Acs Nano* **2013**, *7*, 11272-11282.
2. Haywood, D. G.; Saha-Shah, A.; Baker, L. A.; Jacobson, S. C., Fundamental Studies of Nanofluidics: Nanopores, Nanochannels, and Nanopipets. *Anal Chem* **2015**, *87*, 172-187.
3. Mei, L. J.; Yeh, L. H.; Qian, S. Z., Gate Modulation of Proton Transport in a Nanopore. *Phys Chem Chem Phys* **2016**, *18*, 7449-7458.
4. Mei, L. J.; Yeh, L. H.; Qian, S. Z., Buffer Effect on the Ionic Conductance in a pH-Regulated Nanochannel. *Electrochem Commun* **2015**, *51*, 129-132.
5. Gao, J.; Guo, W.; Feng, D.; Wang, H. T.; Zhao, D. Y.; Jiang, L., High-Performance Ionic Diode Membrane for Salinity Gradient Power Generation. *J Am Chem Soc* **2014**, *136*, 12265-12272.
6. Xiao, K.; Xie, G. H.; Li, P.; Liu, Q.; Hou, G. L.; Zhang, Z.; Ma, J.; Tian, Y.; Wen, L. P.; Jiang, L., A Biomimetic Multi-Stimuli-Response Ionic Gate Using a Hydroxypyrene Derivation-Functionalized Asymmetric Single Nanochannel. *Adv Mater* **2014**, *26*, 6560-6565.
7. Liu, Q.; Xiao, K.; Wen, L. P.; Lu, H.; Liu, Y. H.; Kong, X. Y.; Xie, G. H.; Zhang, Z.; Bo, Z. S.; Jiang, L., Engineered Ionic Gates for Ion Conduction Based on Sodium

- 
- and Potassium Activated Nanochannels. *J Am Chem Soc* **2015**, *137*, 11976-11983.
8. Zhang, H. C.; Hou, X.; Hou, J.; Zeng, L.; Tian, Y.; Li, L.; Jiang, L., Synthetic Asymmetric-Shaped Nanodevices with Symmetric pH-Gating Characteristics. *Adv Funct Mater* **2015**, *25*, 1102-1110.
9. Qiu, Y.; Vlassioux, I.; Chen, Y.; Siwy, Z. S., Direction Dependence of Resistive-Pulse Amplitude in Conically Shaped Mesopores. *Anal Chem* **2016**, *88*, 4917-25.
10. Plett, T.; Shi, W. Q.; Zeng, Y. H.; Mann, W.; Vlassioux, I.; Baker, L. A.; Siwy, Z. S., Rectification of Nanopores in Aprotic Solvents - Transport Properties of Nanopores with Surface Dipoles. *Nanoscale* **2015**, *7*, 19080-19091.
11. Venkatesan, B. M.; Bashir, R., Nanopore Sensors for Nucleic Acid Analysis. *Nat Nanotechnol* **2011**, *6*, 615-624.
12. Kowalczyk, S. W.; Wells, D. B.; Aksimentiev, A.; Dekker, C., Slowing Down DNA Translocation through a Nanopore in Lithium Chloride. *Nano Lett* **2012**, *12*, 1038-1044.
13. Steinbock, L. J.; Lucas, A.; Otto, O.; Keyser, U. F., Voltage-Driven Transport of Ions and DNA through Nanocapillaries. *Electrophoresis* **2012**, *33*, 3480-3487.
14. Lan, W. J.; Kubeil, C.; Xiong, J. W.; Bund, A.; White, H. S., Effect of Surface Charge on the Resistive Pulse Waveshape During Particle Translocation through Glass Nanopores. *J Phys Chem C* **2014**, *118*, 2726-2734.

- 
15. Bell, N. A. W.; Keyser, U. F., Specific Protein Detection Using Designed DNA Carriers and Nanopores. *J Am Chem Soc* **2015**, *137*, 2035-2041.
16. Lan, W. J.; Holden, D. A.; White, H. S., Pressure-Dependent Ion Current Rectification in Conical-Shaped Glass Nanopores. *J Am Chem Soc* **2011**, *133*, 13300-13303.
17. Perera, R. T.; Johnson, R. P.; Edwards, M. A.; White, H. S., Effect of the Electric Double Layer on the Activation Energy of Ion Transport in Conical Nanopores. *J Phys Chem C* **2015**, *119*, 24299-24306.
18. Qiu, Y.; Lin, C. Y.; Hinkle, P.; Plett, T. S.; Yang, C.; Chacko, J. V.; Digman, M. A.; Yeh, L. H.; Hsu, J. P.; Siwy, Z. S., Highly Charged Particles Cause a Larger Current Blockage in Micropores Compared to Neutral Particles. *Acs Nano* **2016**, DOI: 10.1021/acsnano.6b03280.
19. White, H. S.; Bund, A., Ion Current Rectification at Nanopores in Glass Membranes. *Langmuir* **2008**, *24*, 2212-2218.
20. Lin, J. Y.; Lin, C. Y.; Hsu, J. P.; Tseng, S., Ionic Current Rectification in a pH-Tunable Polyelectrolyte Brushes Functionalized Conical Nanopore: Effect of Salt Gradient. *Anal Chem* **2016**, *88*, 1176-1187.
21. Lin, C. Y.; Yeh, L. H.; Hsu, J. P.; Tseng, S., Regulating Current Rectification and Nanoparticle Transport through a Salt Gradient in Bipolar Nanopores. *Small* **2015**,

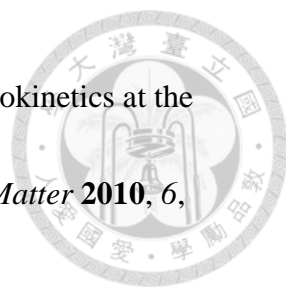
- 
- 11, 4594-4602.
22. Cao, L. X.; Guo, W.; Wang, Y. G.; Jiang, L., Concentration-Gradient-Dependent Ion Current Rectification in Charged Conical Nanopores. *Langmuir* **2012**, 28, 2194-2199.
23. Liu, Q.; Wang, Y.; Guo, W.; Ji, H.; Xue, J.; Ouyang, Q., Asymmetric Properties of Ion Transport in a Charged Conical Nanopore. *Phys Rev E* **2007**, 75.
24. Pu, Q. S.; Yun, J. S.; Temkin, H.; Liu, S. R., Ion-Enrichment and Ion-Depletion Effect of Nanochannel Structures. *Nano Lett* **2004**, 4, 1099-1103.
25. Kubeil, C.; Bund, A., The Role of Nanopore Geometry for the Rectification of Ionic Currents. *J Phys Chem C* **2011**, 115, 7866-7873.
26. Vlassioug, I.; Smirnov, S.; Siwy, Z., Ionic Selectivity of Single Nanochannels. *Nano Lett* **2008**, 8, 1978-1985.
27. Dai, J. H.; Ito, T.; Sun, L.; Crooks, R. M., Electrokinetic Trapping and Concentration Enrichment of DNA in a Microfluidic Channel. *J Am Chem Soc* **2003**, 125, 13026-13027.
28. Siwy, Z.; Fulinski, A., Fabrication of a Synthetic Nanopore Ion Pump. *Phys Rev Lett* **2002**, 89.
29. Yeh, L. H.; Hughes, C.; Zeng, Z. P.; Qian, S. Z., Tuning Ion Transport and Selectivity by a Salt Gradient in a Charged Nanopore. *Anal Chem* **2014**, 86, 2681-



- 2686.
30. Cervera, J.; Schiedt, B.; Neumann, R.; Mafe, S.; Ramirez, P., Ionic Conduction, Rectification, and Selectivity in Single Conical Nanopores. *J Chem Phys* **2006**, *124*.
31. Tseng, S.; Li, Y. M.; Lin, C. Y.; Hsu, J. P., Salinity Gradient Power: Influences of Temperature and Nanopore Size. *Nanoscale* **2016**, *8*, 2350-2357.
32. Zeng, Z. P.; Yeh, L. H.; Zhang, M. K.; Qian, S. Z., Ion Transport and Selectivity in Biomimetic Nanopores with pH-Tunable Zwitterionic Polyelectrolyte Brushes. *Nanoscale* **2015**, *7*, 17020-17029.
33. Cervera, J.; Ramirez, P.; Mafe, S.; Stroeve, P., Asymmetric Nanopore Rectification for Ion Pumping, Electrical Power Generation, and Information Processing Applications. *Electrochim Acta* **2011**, *56*, 4504-4511.
34. Hou, X.; Zhang, H. C.; Jiang, L., Building Bio-Inspired Artificial Functional Nanochannels: From Symmetric to Asymmetric Modification. *Angew Chem Int Edit* **2012**, *51*, 5296-5307.
35. Haywood, D. G.; Harms, Z. D.; Jacobson, S. C., Electroosmotic Flow in Nanofluidic Channels. *Anal Chem* **2014**, *86*, 11174-11180.
36. Laohakunakorn, N.; Keyser, U. F., Electroosmotic Flow Rectification in Conical Nanopores. *Nanotechnology* **2015**, *26*.
37. Daiguji, H., Ion Transport in Nanofluidic Channels. *Chem Soc Rev* **2010**, *39*, 901-



- 911.
38. Ai, Y.; Zhang, M. K.; Joo, S. W.; Cheney, M. A.; Qian, S. Z., Effects of Electroosmotic Flow on Ionic Current Rectification in Conical Nanopores. *J Phys Chem C* **2010**, *114*, 3883-3890.
39. Lin, D. H.; Lin, C. Y.; Tseng, S.; Hsu, J. P., Influence of Electroosmotic Flow on the Ionic Current Rectification in a pH-Regulated, Conical Nanopore. *Nanoscale* **2015**, *7*, 14023-14031.
40. Besteman, K.; Zevenbergen, M. A. G.; Lemay, S. G., Charge Inversion by Multivalent Ions: Dependence on Dielectric Constant and Surface-Charge Density. *Phys Rev E* **2005**, *72*.
41. van der Heyden, F. H. J.; Stein, D.; Besteman, K.; Lemay, S. G.; Dekker, C., Charge Inversion at High Ionic Strength Studied by Streaming Currents. *Phys Rev Lett* **2006**, *96*.
42. Prakash, S.; Zambrano, H. A.; Rangharajan, K. K.; Rosenthal-Kim, E.; Vasquez, N.; Conlisk, A. T., Electrokinetic Transport of Monovalent and Divalent Cations in Silica Nanochannels. *Microfluid Nanofluid* **2016**, *20*.
43. He, Y.; Gillespie, D.; Boda, D.; Vlassiouk, I.; Eisenberg, R. S.; Siwy, Z. S., Tuning Transport Properties of Nanofluidic Devices with Local Charge Inversion. *J Am Chem Soc* **2009**, *131*, 5194-5202.

- 
44. Aguilera-Arzo, M.; Calero, C.; Faraudo, J., Simulation of Electrokinetics at the Nanoscale: Inversion of Selectivity in a Bio-Nanochannel. *Soft Matter* **2010**, *6*, 6079-6082.
45. Garcia-Gimenez, E.; Alcaraz, A.; Aguilera, V. M., Overcharging Below the Nanoscale: Multivalent Cations Reverse the Ion Selectivity of a Biological Channel. *Phys Rev E* **2010**, *81*.
46. Valisko, M.; Boda, D., Selective Adsorption of Ions with Different Diameter and Valence at Highly Charged Interfaces. *J Phys Chem C* **2007**, *111*, 15575-15585.
47. Keh, H. J.; Huang, T. Y., Diffusiophoresis and Electrophoresis of Colloidal Spheroids. *J Colloid Interf Sci* **1993**, *160*, 354-371.
48. Piguet, F.; Discala, F.; Breton, M. F.; Pelta, J.; Bacri, L.; Oukhaled, A., Electroosmosis through Alpha-Hemolysin That Depends on Alkali Cation Type. *J Phys Chem Lett* **2014**, *5*, 4362-4367.
49. Bhattacharya, S.; Muzard, J.; Payet, L.; Mathe, J.; Bockelmann, U.; Aksimentiev, A.; Viasnoff, V., Rectification of the Current in Alpha-Hemolysin Pore Depends on the Cation Type: The Alkali Series Probed by Molecular Dynamics Simulations and Experiments. *J Phys Chem C* **2011**, *115*, 4255-4264.
50. Gamble, T.; Decker, K.; Plett, T. S.; Pevarnik, M.; Pietschmann, J. F.; Vlassioux, I.; Aksimentiev, A.; Siwy, Z. S., Rectification of Ion Current in Nanopores Depends on



- the Type of Monovalent Cations: Experiments and Modeling. *J Phys Chem C* **2014**, *118*, 9809-9819.
51. Liu, J.; Kvetny, M.; Feng, J.; Wang, D.; Wu, B.; Brown, W.; Wang, G., Surface Charge Density Determination of Single Conical Nanopores Based on Normalized Ion Current Rectification. *Langmuir* **2012**, *28*, 1588-95.
52. Liu, M. Y.; Zhang, H. C.; Li, K.; Heng, L. P.; Wang, S. T.; Tian, Y.; Jiang, L., A Bio-Inspired Potassium and pH Responsive Double-Gated Nanochannel. *Adv Funct Mater* **2015**, *25*, 421-426.
53. Yeh, H. C.; Chang, C. C.; Yang, R. J., Electro-Osmotic Pumping and Ion-Concentration Polarization Based on Conical Nanopores. *Phys Rev E* **2015**, *91*.
54. Tseng, S.; Lin, S. C.; Lin, C. Y.; Hsu, J. P., Influences of Cone Angle and Surface Charge Density on the Ion Current Rectification Behavior of a Conical Nanopore. *J Phys Chem C* **2016**, *120*, 25620–25627.
55. Siwy, Z.; Heins, E.; Harrell, C. C.; Kohli, P.; Martin, C. R., Conical-Nanotube Ion-Current Rectifiers: The Role of Surface Charge. *J Am Chem Soc* **2004**, *126*, 10850-10851.



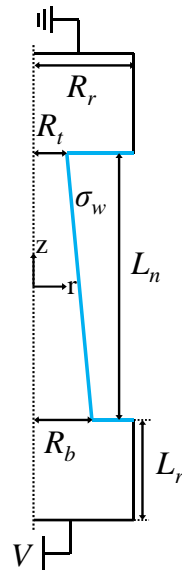


**Figure 1-1.** Schematic of a conical nanopore with  $L_n=1000$  nm,  $R_t=5$  nm,  $R_b=28$  nm, half cone angle  $\theta=1.32^\circ$ ,  $L_r=R_r=800$  nm, and  $\sigma_w=-1$  e/nm<sup>2</sup>.

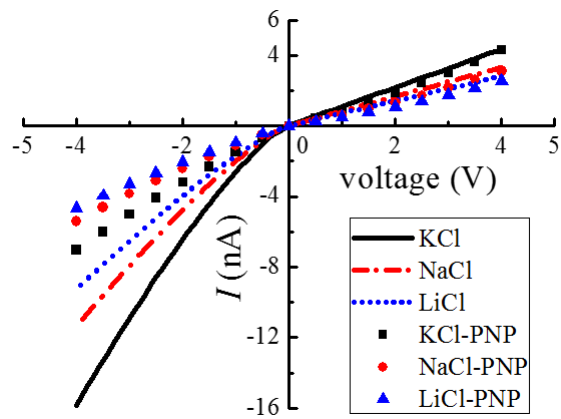


**Figure 1-2.** Current-voltage curves of a conical nanopore for various types of salt with and without considering EOF at  $C_0=50$  mM. Black solid curve: KCl, (PNP+NS) model; open squares: KCl, PNP model. Red dashed curve: NaCl, (PNP+NS) model; open circles: NaCl, PNP model. Blue dotted curve: (PNP+NS) model; open triangles: LiCl, PNP model.

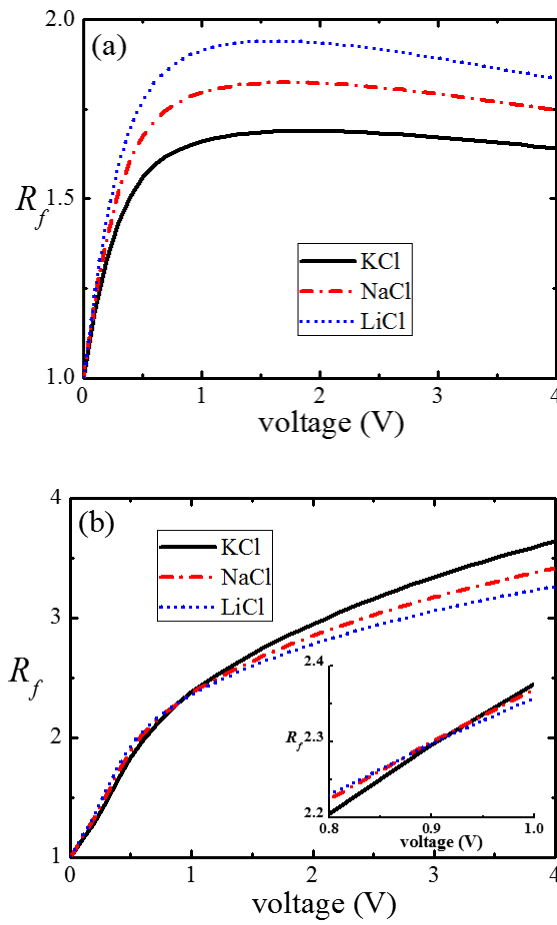


**Figure 1-3.** Variation of the current rectification factor  $R_f$  with applied voltage bias  $V$  for various types of salt at  $C_0=50$  mM. (a) PNP model, (b) (PNP+NS) model.

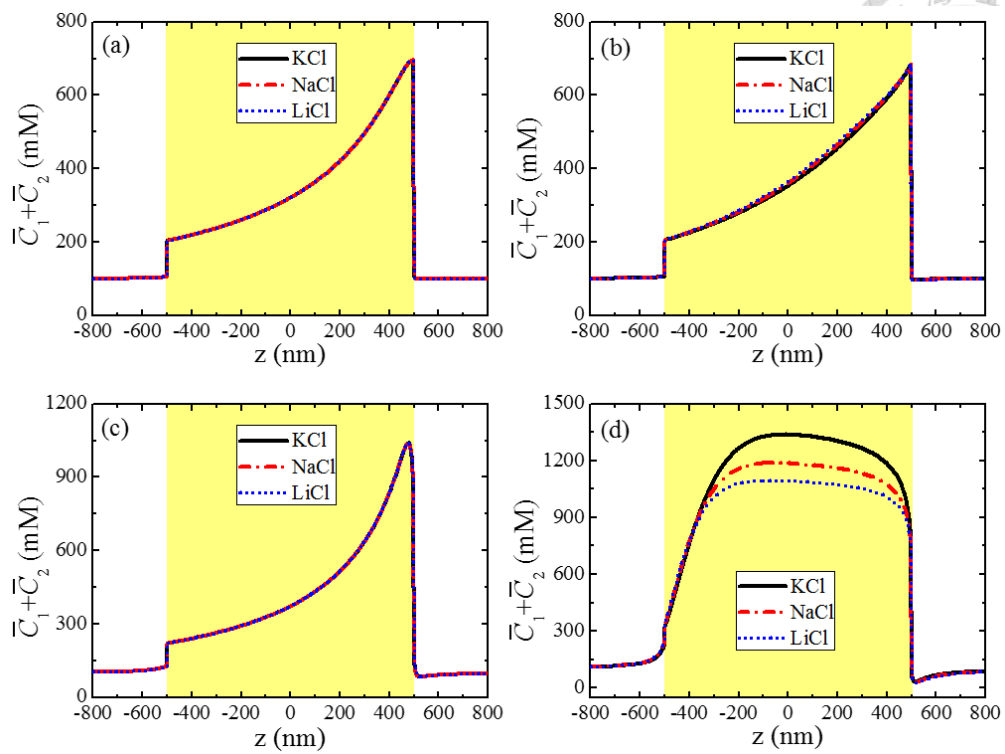


**Figure 1-4.** Axial variation in the cross sectional averaged concentrations under various conditions at  $C_0=50$  mM. (a) PNP model at  $V=-0.2$ V, (b) (PNP+NS) model at  $V=-0.2$ V, (c) PNP model at  $V=-2$ V, (d) (PNP+NS) model at  $V=-2$ V.

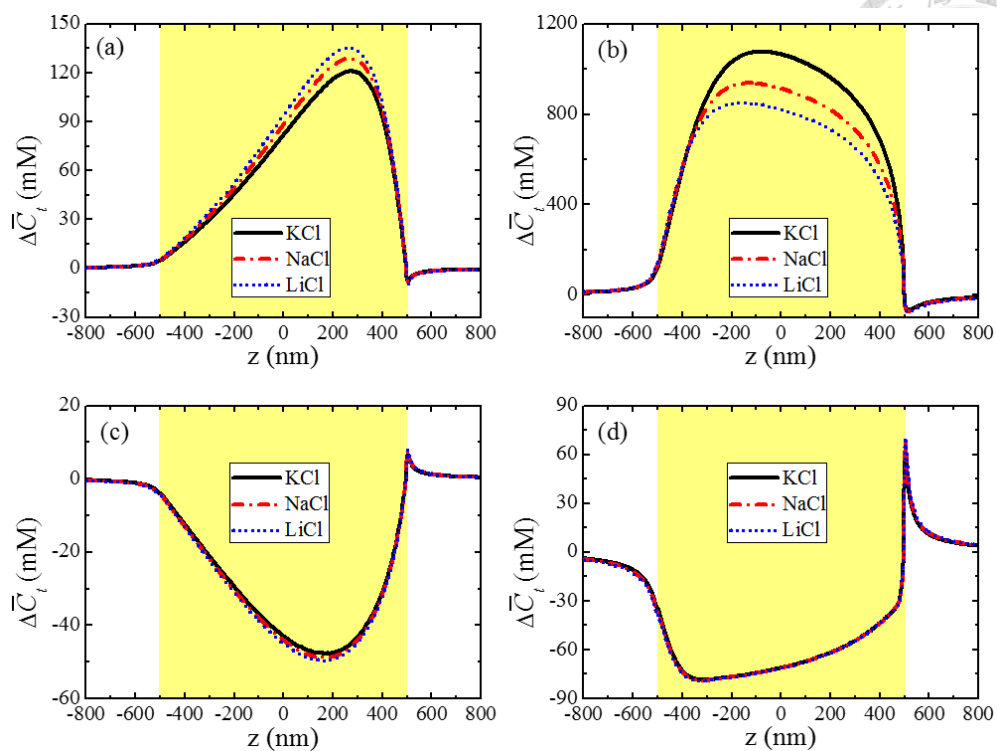


**Figure 1-5.** Axial variations in the cross sectional averaged concentration difference at various levels of the applied bias for the present (PNP+NS) model. (a)  $V = -0.2$  V, (b)  $V = -2$  V, (c)  $V = 0.2$  V, (d)  $V = 2$  V.

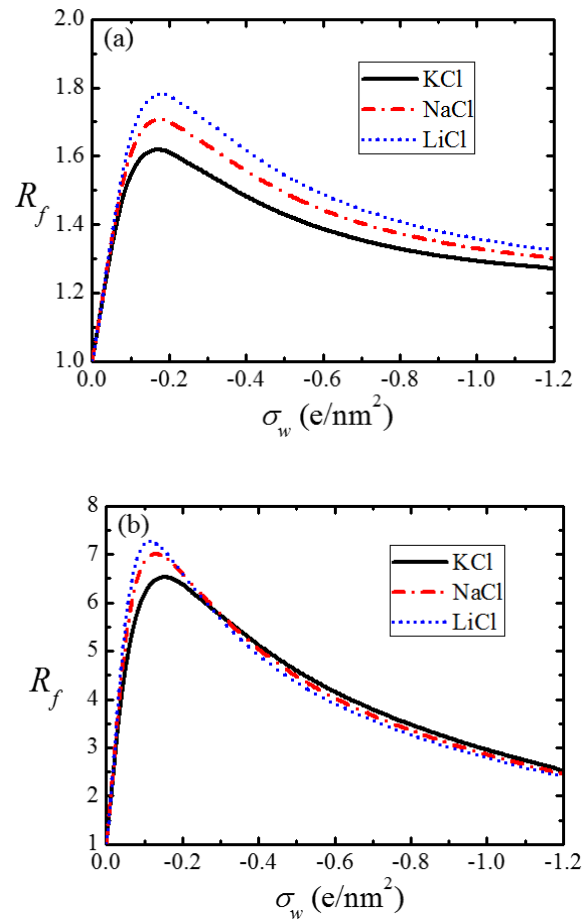


**Figure 1-6.** Variation of the current rectification factor  $R_f$  with surface charge density

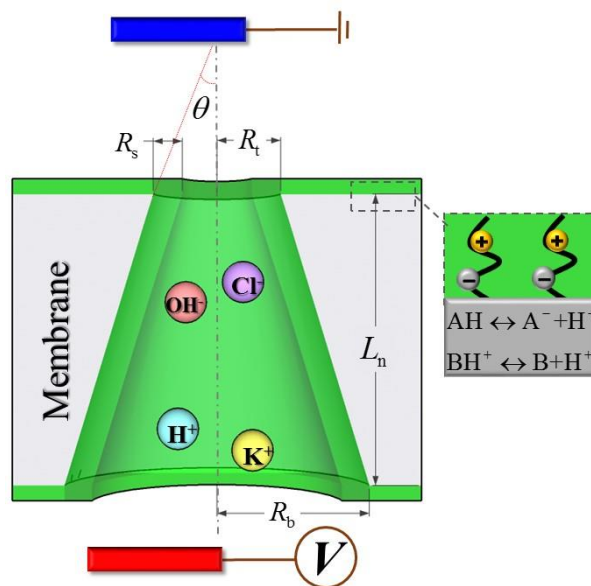
$\sigma_w$  for various types of salt at  $C_0=50$  mM. (a)  $|V|=0.2$  V, (b)  $|V|=2$  V.

# CHAPTER 2: Effect of polyelectrolyte functionalized surface



## Ion Transport and Selectivity in a Conical Nanopore Functionalized with pH-

### Tunable Polyelectrolyte Brushes





## 2-1. Introduction

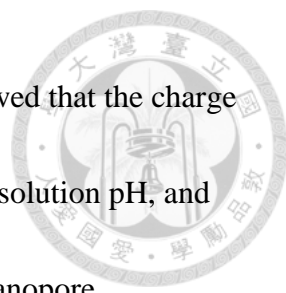
Ion current rectification (ICR) and ion selectivity are two specific and interesting electrokinetic behaviors of a nanopore. These behaviors have been studied both theoretically<sup>1-4</sup> and experimentally<sup>5-10</sup> in many recent works. ICR is a nonlinear diode-like current voltage behavior occurring when the linear size of a charged nanopore is comparable to the thickness of the associated electric double layer (EDL). ICR was proposed to arise from the overlapping of the nanopore EDL causing an asymmetric transport of cations and anions so that ion depletion/enrichment occurs when an applied electric bias is switched.<sup>11</sup> ICR is influenced by both the geometry of a nanopore and the salt concentration.<sup>12-14</sup> Adopting a model comprising Poisson and Nernst-Planck (PNP) equations, Wang *et al.*<sup>15</sup> examined the factors influencing the ICR behavior of both conical and bullet shaped nanopores Daiguji *et al.*<sup>16</sup> investigated the ion transport in a silica nanochannel with a gate electrode embedded in its middle region. Based on a PNP model, they concluded that the ion transport in the nanochannel is influenced significantly by the surface charge density. Ai *et al.*<sup>17</sup> studied the influence of EOF on ICR in a conical nanopore by solving coupled PNP and Navier-Stokes (PNP+NS) equations. They found that the EOF effect is most significant when the applied potential bias is high and both the surface charge density and the EDL thickness take a medium large value. Chen *et al.*<sup>18</sup> concluded that the electroosmotic velocity in a pH-tunable



nanochannel is slower than that in a nanochannel having constant surface charge density.



Recently, surface modified nanopores are used widely in various applications including sensing devices.<sup>19-22</sup> For example, PET and glass nanopores are grafted with polyelectrolytes (PEs), proteins, and antibodies so that they can be regulated by external stimuli such as pH.<sup>20, 23-30</sup> This is inspired by the pH regulated nature of biological ion channels<sup>31-32</sup>. For instance, adopting a polyimide asymmetric nanochannel with its surface modified by amphoteric chains, Ali *et al.*<sup>33</sup> showed that its rectification property is pH-tunable. Using a DNA modified PET membrane Liu *et al.*<sup>34</sup> prepared a potassium and pH responsive double-gated nanochannel. They showed that through applying proper stimuli (pH and potassium concentration) and adjusting the gate status (open or close), ICR phenomenon can be observed. Adopting a PNP-NS model, Zeng *et al.*<sup>35</sup> studied the ICR behavior of a conical nanopore having pH-regulated polyelectrolyte (PE) brushes. They concluded that this behavior is most significant when both the PE charge density and the bulk salt concentration take a medium value. Taking account of an additionally applied salt gradient, the same system was investigated by Lin *et al.*<sup>36</sup> They found that the ICR behavior depends on the charge density of the PE layer, the solution pH, and the thickness of EDL, and its behavior can be explained by the distribution of ions and the local electric field near the nanopore tip. In a study of the



ionic transport in a PE-modified straight nanopore, Zeng *et al.*<sup>37</sup> showed that the charge density of the PE layer is affected by the bulk salt concentration, the solution pH, and the grafting density, yielding profound transport phenomena in the nanopore.

Nanopores can also behave as an ion filter. For example, in a study of sodium ion channels, Dudev *et al.*<sup>38</sup> found that the selectivity of an ion channel is affected by its structure and the amount and types of protein-ligand inside. Vlassioux *et al.*<sup>39</sup> analyzed theoretically the selectivity of a nanochannel having fixed charged, and concluded that to achieve the largest selectivity, a long, thin nanochannel having high charged walls should be chosen. Applying a PNP-NS model, Yeh *et al.*<sup>40</sup> discussed the ion selectivity in a nanopore having constant charge density with a salt gradient imposed. It was shown that the ion selectivity of the nanopore can be tuned by adjusting the strengths of simultaneously applied electric field and salt concentration gradient.

This study is aimed to investigate both the ion transport behaviors and ion selectivity in a conical nanopore functionalized with a PE layer. Generalizing previous studies, a PNP-NS model is adopted and the effect of EOF is examined in detail. In addition, the PE layer is pH-tunable so that its charged conditions are more realistic compared to, for example, that of solid state nanopores having a constant charge density. Furthermore, compared to symmetric nanochannels, the specific geometry of the conical nanopore considered is able to influence the direction of the applied electric

field, yielding profound and interesting phenomena, such as ion enrichment/depletion.

This in turn, will affect the ion transport behavior of the nanopore, including its conductance, ionic current, and ion selectivity. The influences of the applied potential bias, the bulk salt concentration, and pH on the system under consideration are examined and the underlying mechanisms discussed.

## 2-2. Theoretical Model

Let us consider the transport of ions in the system shown in Figure 2-1, where two identical, large reservoirs of axial length  $L_R$  and radius  $R_R$  are connected by a conical nanopore of axial length  $L_N$ , tip radius  $R_T$ , and base radius  $R_B$  embedded in a membrane. The nanopore surface and the reservoir walls near the nanopore openings are grafted with a pH-tunable polyelectrolyte (PE) brush layer of thickness  $R_s$ . The system is filled with an incompressible, aqueous salt solution. Suppose that the reservoirs are large, so that the salt concentration at a point sufficient far away from the nanopore openings reaches the bulk value. A potential bias  $V$  is applied across the nanopore, driving ions from reservoir to the other, and an ionic current is induced. The cylindrical coordinates with the radial and axial distances  $r$  and  $z$ , respectively, and the origin at the nanopore center system are adopted.

We assume that the PE considered has two types of functional group, AH and B,



having the following dissociation/association reactions:



Let  $K_A = [A^-][H^+]/[AH]$  and  $K_B = [B][H^+]/[BH^+]$  be the equilibrium constants of these

reactions, where  $[ \bullet ]$  is the molar concentration of species  $\bullet$ . Let  $N_A$  and  $N_B$  be the total

concentrations of AH and B, respectively. Then,

$$N_A = [A^-] + [AH] = [A^-] \left( 1 + \frac{[H^+]}{K_A} \right) \quad (2-2)$$

$$N_B = [B] + [BH^+] = [BH^+] \left( 1 + \frac{K_B}{[H^+]} \right) \quad (2-2a)$$

Therefore, if  $F$  is Faradays constant, the charge density (Coul/m<sup>3</sup>) of the PE layer is

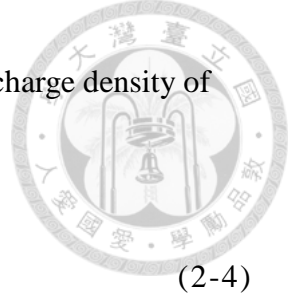
$$\rho_{PE} = 1000F ([BH^+] - [A^-]) = 1000F \left( \frac{N_B [H^+]}{K_B + [H^+]} - \frac{N_A K_A}{K_A + [H^+]} \right) \quad (2-3)$$

Suppose that the background salt in the liquid phase is KCl and the solution pH is adjusted by KOH and HCl. Therefore, four types of ionic species are present: H<sup>+</sup>, OH<sup>-</sup>, K<sup>+</sup>, and Cl<sup>-</sup>. Let  $C_{j0}$  be the bulk concentration of species  $j$ ; the possible values of  $j$  are 1, 2, 3, and 4, corresponding to K<sup>+</sup>, Cl<sup>-</sup>, H<sup>+</sup>, and OH<sup>-</sup>, respectively. If  $C_b$  is the background concentration of KCl, then due to electroneutrality, the following relationships apply:

$$C_{10} = C_b, \quad C_{20} = C_b + 10^{-(pH+3)} - 10^{-(14-pH)+3}, \quad C_{30} = 10^{-(pH+3)}, \quad \text{and} \quad C_{40} = 10^{-(14-pH)+3} \quad \text{for}$$

$$pH \leq 7; \quad C_{10} = C_b - 10^{-(pH+3)} + 10^{-(14-pH)+3}, \quad C_{20} = C_b, \quad C_{30} = 10^{-(pH+3)}, \quad \text{and}$$

$$C_{40} = 10^{-(14-pH)+3} \quad \text{for} \quad pH \geq 7.$$



Letting  $\varepsilon$  be the fluid permittivity and  $\rho_e = \sum_{j=1}^4 Fz_j C_j$  the space charge density of mobile ions, the electric potential  $\phi$  is described by

$$\nabla^2 \phi = -\frac{\rho_e + h\rho_{PE}}{\varepsilon} \quad (2-4)$$

$h$  is 0 for the region outside the PE layer, and 1 for that inside the PE layer.

The conservation of ionic species  $j$  yields the Poisson-Nernst-Planck (PNP) equation

$$\nabla \cdot \mathbf{N}_j = \nabla \cdot \left( C_j \mathbf{u} - D_j \nabla C_j - z_j \frac{D_j}{RT} FC_j \nabla \phi \right) = 0, j=1,2,3,4 \quad (2-5)$$

$\mathbf{N}_j$ ,  $C_j$ ,  $D_j$ , and  $z_j$  denote the flux, the concentration, the diffusion coefficient, and the valence of ionic species  $j$ .  $\mathbf{u}$ ,  $F$ ,  $R$ , and  $T$  are the fluid velocity, Faraday constant, gas constant, and the absolute temperature, respectively.

Assuming steady state, the flow field in the present case is described by the equation of continuity and the modified Stokes-Brinkman equation

$$\nabla \cdot \mathbf{u} = 0 \quad (2-6)$$

$$-\nabla p + \eta \nabla^2 \mathbf{u} - \rho_e \nabla \phi - h\gamma \mathbf{u} = \mathbf{0} \quad (2-7)$$

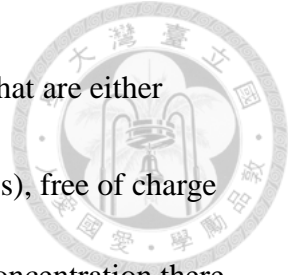
$\eta$ ,  $p$ , and  $\gamma$  are the fluid viscosity, the hydrodynamic pressure, and the hydrodynamic frictional coefficient of the PE layer, respectively.

The ionic current  $I$  through the nanopore can be calculated by

$$I = \int_A F \left( \sum_{j=1}^4 z_j \mathbf{N}_j \right) \cdot \mathbf{n} dA, \quad (2-8)$$

where  $A$  is the surface of either reservoir end normal to the nanopore axis.

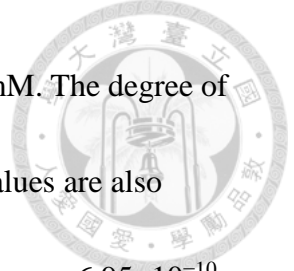
To specify the boundary conditions associated with Eqs. (4)-(7), we assume the



following: (i) The surfaces sufficiently from the nanopore openings that are either perpendicular or parallel to the nanopore axis are slip ( $\mathbf{u}$  is continuous), free of charge ( $\mathbf{n} \cdot \nabla \phi = 0$ ), and free of ionic flux ( $\mathbf{n} \cdot \mathbf{N}_j = 0$ ). In addition, the ion concentration there reaches essentially the bulk value ( $C_j = C_{j0}$ ),  $\phi(z=L_R) = 0$ , and  $\phi(z=-L_N - L_R) = V$ . (ii) The rigid surface of the membrane wall is impermeable to ions ( $\mathbf{n} \cdot \mathbf{N}_j = 0$ ), no slip ( $\mathbf{u} = \mathbf{0}$ ), and free of charge, ( $\mathbf{n} \cdot (\epsilon \nabla \phi) = 0$ ). (iii) No external pressure is applied across the two reservoirs ( $p = 0$ ). Note that, due to axial symmetry, all dependent variables are azimuthal angle independent. Because the ion radius (0.03-0.2 nm) is much smaller than the nanopore size, the effect of ionic volume is neglected in this study, for simplicity.

### 2-3. Results and Discussions

Our model is solved numerically by COMSOL Multiphysics (version 4.3a, <http://www.comsol.com>), and a detailed numerical simulation is conducted to examine the behavior of the system under consideration by varying the solution pH, the background salt concentration  $C_b$ , and the applied potential bias  $V$ . To this end, we assume  $L_n = 1000$  nm,  $R_t = 8$  nm,  $R_b = 95.5$  nm,  $L_r = R_r = 400$  nm,  $R_s = 4$  nm, and the half cone angle  $\theta = 5^\circ$ . For illustration, we consider a lysine PE layer of  $pK_A = 2.2$  ( $\alpha$ -carboxylic groups),  $pK_B = 9$  ( $\alpha$ -amino groups), so that the isoelectric point (IEP) of the PE layer is 5.6. Since the grafting density of biological PEs is on the order of 0.1 chains/nm<sup>2</sup>,<sup>41</sup> we

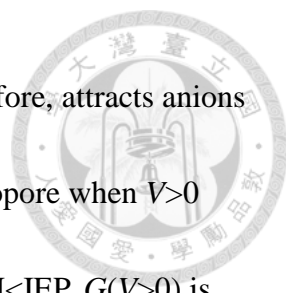


assume  $\sigma_m=0.1$  PE chains/nm<sup>2</sup>, and therefore,  $N_A=N_B=\sigma_m/R_s=41.67$  mM. The degree of softness of the PE layer  $\lambda^{-1}=(\eta/\gamma)$  is fixed at 1 nm.<sup>42</sup> The following values are also adopted:  $F=96500$  Coul/mol,  $R=8.314$  J/mol K,  $T=298$  K,  $\mu=0.001$  Pa s,  $\varepsilon=6.95\times 10^{-10}$  F/m,  $D_1=D_{K^+}=1.96\times 10^{-9}$  m<sup>2</sup>/s,  $D_2=D_{Cl^-}=2.03\times 10^{-9}$  m<sup>2</sup>/s,  $D_3=D_{H^+}=9.38\times 10^{-9}$  m<sup>2</sup>/s, and  $D_4=D_{OH^-}=5.29\times 10^{-9}$  m<sup>2</sup>/s.

Figure 2-2 illustrates the variation in the nanopore conductance  $G$  defined below with the solution pH, level of applied potential bias  $V$ , and the bulk salt concentration  $C_b$ :

$$G = \frac{I}{V} = \frac{\int_A F \left( \sum_{j=1}^4 z_j \mathbf{N}_j \right) \cdot \mathbf{n} dA}{V} \quad (2-9)$$

is the surface of either reservoir end normal to the axis of the nanopore. Figure 2-2(a) reveals that if  $V>0$  and  $C_b$  is low (1 mM),  $G$  shows a local minimum at the IEP (pH 5.6) of the PE layer. This is because the more the pH deviates from the IEP the more complete the dissociation of the functional groups of this layer, yielding a higher charge density, so that a more amount of counterions is attracted into the nanopore and, therefore, a larger  $G$ . However, if  $C_b$  is raised to 100 mM,  $G$  decreases with increasing pH, in general. In contrast, as seen in Figure 2-2(b), if  $V<0$ , the behavior of  $G$  at low  $C_b$  (1 mM) is the same as that when  $V>0$ . It is interesting to observe that if  $C_b$  is raised to 100 mM,  $G$  has a local minimum as pH varies, which is quite different from that when  $V>0$ . This can be explained by the effect of ion concentration polarization (ICP). If pH



is lower than IEP (5.6), the nanopore is positively charged, and therefore, attracts anions into the nanopore so that ion enrichment/depletion occurs in the nanopore when  $V>0$  ( $V<0$ ). A comparison between Figure 2-2(a) and (b) reveals that if  $\text{pH}<\text{IEP}$ ,  $G(V>0)$  is larger than  $G(V<0)$ . In contrast, if  $\text{pH}$  is higher than IEP, the PE layer is negatively charged so that cations are attracted into the nanopore. In this case, ion enrichment occurs when  $V<0$ , and depletion occurs when  $V>0$ . As seen in Figure 2-2, if  $\text{pH}$  exceeds IEP,  $G(V<0)$  is larger than  $G(V>0)$ . As  $\text{pH}$  gets close to IEP,  $G$  becomes insensitive to both the direction and the magnitude of  $V$ . This is because the PE layer of the nanopore is nearly free of charged in this case so that the ICR effect is not important<sup>17</sup>, and therefore,  $G$  depends mainly on  $C_b$ .

Figure 2-2 suggests that the variation of  $G$  with  $\text{pH}$  at a low  $C_b$  is more appreciable than that at a high  $C_b$ . For instance, as seen in Table 2-1 that the degree of increase in  $G$  as  $\text{pH}$  is lowered from 6 to 2 at  $C_b=1$  mM is much larger than that at  $C_b=100$  mM. That is, the value of  $G$  at a low salt concentration is more sensitive to the change in  $\text{pH}$ . As  $C_b$  decreases, the thickness of electrical double layer increases, so that its overlap near the nanopore tip can be significant. As pointed out by Ma *et al.*<sup>43</sup> that in this case the conductance of the nanopore is influenced mainly by its surface property. As  $\text{pH}$  deviates from the IEP of the PE layer, its surface charge density increases accordingly. Therefore, the variation of  $G$  with  $\text{pH}$  at low  $C_b$  is more appreciable than that at high  $C_b$ .





Figure 2-2 also reveals that the conductance of the nanopore is affected by the level of the applied potential bias  $V$ . Figure 2-2(a) indicates that if pH is significantly lower than the IEP of the PE layer, the degree of ion enrichment increases with  $V$ , so is the conductance  $G$ . In contrast, if pH exceeds IEP, the degree of ion depletion increases with  $V$ , yielding a decrease in  $G$ . The direction of  $V$  in Figure 2-2(b) is opposite to that in Figure 2(a).

Note that at  $C_b=100$  mM,  $G$  is insensitive to the variation of pH for pH ranging from 10 to 12, which is not the case at  $C_b=1$  mM. To explain this, we plot the variation of the volume averaged charge density of the PE layer  $\rho_a^*$  defined below with pH for the case of Figure 2-3:

$$\rho_a^* = \frac{\int_{\Omega_{PE}} \rho^* d\Omega_{PE}}{\int_{\Omega_{PE}} d\Omega_{PE}}, \quad (2-10)$$

where  $\Omega_{PE}$  is the volume of the PE layer.  $\rho_a^*$  is influenced mainly by pH and  $C_b$ , and is insensitive to the applied potential bias. At  $C_b=100$  mM, because the dissociation of the PE layer is almost complete at pH 10, so that if pH>10,  $\rho_a^*$ , and therefore,  $G$  remains roughly the same for 10<pH<11. However, if pH>11, the concentration of OH<sup>-</sup> is appreciable, so is its contribution to  $G$ , thereby raising  $G$ . Note also that the surface charge density (or the degree of dissociation of the functional groups) of the PE layer of the nanopore varies with  $C_b$ . As  $C_b$  increases, more amount of K<sup>+</sup> are attracted by the nanopore surface, the concentration of H<sup>+</sup> decreases accordingly, so that the PE layer is




more negatively charged.

To further explain the variation in the nanopore conductance  $G$ , we plot the axial variations in the cross-sectional averaged ionic concentrations  $C_{a,i}$  defined below for various levels of pH in Figures 2-4 to 2-6:

$$C_{a,j} = \frac{\int_{\Lambda} C_j d\Lambda}{\int_{\Lambda} d\Lambda}, \quad (2-11)$$

where  $\Lambda$  is the cross-sectional area of the nanopore, which is  $z$ -dependent, and  $C_j$  the concentration of ionic species  $j$ .

In Figure 2-4, pH is 3 so that the PE layer of the nanopore is positively charged. In this case, anions are attracted into the nanopore and, due to double layer overlapping, their concentration shows a local maximum near the nanopore tip region. If  $V > 0$  (Figure 2-4(a) and (c)), anions (cations) are driven from the nanopore tip (base) end to its base (tip) end,. In this case both anions and cations are enriched in the nanopore, thereby raising its conductance  $G$ . As  $V$  is raised from 0.3 to 1 V, the degree of enrichment, and therefore,  $G$  increases accordingly. Also, the position at which the peak value of  $C_{a,j}$  occurs shifts slightly from the nanopore tip into its interior. Note that the higher the  $V$  the more significant the ion concentration polarization (ICP), as can be inferred from the difference in the maximum and the minimum values of  $C_{a,j}$ , implying that the higher the  $V$  the more significant the effects of ion enrichment/depletion. In contrast, if  $V < 0$



(Figure 2-4(b) and (d)), anions (cations) are driven from the nanopore base (tip) end to its tip (base) end. In this case, the depletion of both cations and anions occurs in the nanopore so that the  $G$  is smaller than that for the case of  $V > 0$ . Therefore, the current for  $V > 0$  is larger than that for  $V < 0$ , known as the phenomenon of ionic current rectification.<sup>1</sup> Figure 2-4 reveals that although the increase in the cross-sectional averaged ion concentration at  $C_b = 100$  mM as  $V$  increases is more appreciable than that at  $C_b = 1$  mM, the degree of ion concentration polarization in the latter is more significant than that in the former. This is because the lower the  $C_b$  the thicker the double layer and the more significant its overlapping.

The pH in Figure 2-5 (6) is close to the IEP of the PE layer of the nanopore (5.6) so that it is only slightly negatively charged, as seen in Figure 2-3, and therefore, the concentration of cations is higher than that of anions in the nanopore. Figure 2-5 reveals that the weakly charged PE layer yields a weak ion enrichment/depletion in the nanopore. Therefore, the nanopore conductance remains almost constant if pH is around IEP so that the ICR effect is inappreciable. This is in agree with that the ICR effect comes from not only the asymmetric geometry of a nanopore but also its charge density.

Figure 2-6 shows the axial variation in the cross-sectional averaged ionic concentrations  $C_{a,i}$  at pH 9. In this case, the PE layer of the nanopore is negatively charged, as seen in Figure 2-3, so that more cations are present in the nanopore than



anions. If  $V < 0$  (Figure 2-6(b) and 2-6(d)), both cations and anions are enriched inside the nanopore. As  $V$  varies from  $-0.3$  V to  $-1$  V, the degree of ion enrichment becomes more significant at both  $C_b = 1$  mM and  $C_b = 100$  mM, but is more apparent in the latter.

Therefore, if  $\text{pH} > \text{IEP}$ , the increase of  $G(C_b = 100 \text{ mM})$  with increasing  $|V|$  is more apparent than that of  $G(C_b = 1 \text{ mM})$ . The profile of  $C_{a,i}$  at pH 3 suggests that the ICP phenomena at  $C_b = 1$  mM is more significant than that at  $C_b = 100$  mM. If  $V > 0$  (Figure 2-6(a) and 2-6(c)), the concentration profile at  $C_b = 1$  mM is quite different from that at  $C_b = 100$  mM. In the former (Figure 2-5(a)), cations are depleted and anions enriched inside the nanopore with most of them confined in the PE layer of the nanopore.

However, both anions and cations are depleted inside the nanopore in the latter (Figure 2-5(c) and Figure 2-7(a)). This explains that if  $\text{pH} > \text{IEP}$ ,  $G$  decreases with increasing pH at  $C_b = 100$  mM, but increases with increasing pH at  $C_b = 1$  mM. A comparison between Figure 2-7(c) (pH 2.2) and Figure 2-7(b) (pH 9) reveals that although the deviations of the solution pH from IEP are the same in these two cases, the corresponding concentration profiles are quite different. This is because the charge density of the PE layer at pH 9 is higher than that at pH 2.2, and the bulk salt concentration is sufficiently low so that most of cations are confined in the PE layer of the nanopore.

To further examine the transport properties of the present conical nanopore, we plot the variation of its selectivity  $S$  with pH in Figure 2-8. If we let  $I_+ = I_1 + I_3$  and



$I_- = I_2 + I_4$  be the ionic current contributed by cations and that by anions, respectively,

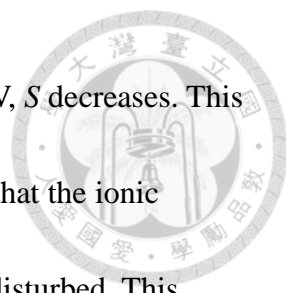
then

$$S = \frac{|I_+| - |I_-|}{|I_+| + |I_-|} \quad (2-12)$$

Note that  $S > 0$  for a cation-selective nanopore, and  $S < 0$  for an anion-selective nanopore.

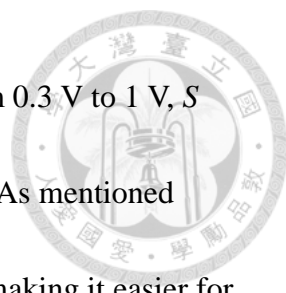
Figure 2-8 reveals that the variation of  $S$  with pH at  $C_b = 1$  mM is more sensitive than that at  $C_b = 100$  mM,  $S(C_b = 1 \text{ mM})$  is larger than  $S(C_b = 100 \text{ mM})$ , in general. This is because the lower the  $C_b$  the thicker the EDL, and the more significant the EDL overlapping near the nanopore tip region the more difficult for ions to pass through so that counterions are enriched and coions depleted, and  $S$  deviates more from zero. If pH is close to IEP, the nanopore is nearly uncharged so that  $S \cong 0$ .

The conical nanopore is negatively (positively) charged for  $\text{pH} > \text{IEP}$  ( $\text{pH} < \text{IEP}$ ) and, therefore, is cation- (anion-) selective. Figure 2-8 reveals that if  $\text{pH} > \text{IEP}$ ,  $S$  has a local maximum, and can become negative if pH is sufficiently high. This is because the charge density of the PE layer increases with increasing pH so that it attracts more cations into the nanopore and  $S$  increases accordingly. However, if pH is sufficiently high, the presence of  $\text{OH}^-$  can be more significant than that of cations so that the nanopore becomes anion-selective. This can be shown in Figure 2-9, where the ionic flux of each species is presented. As can be seen in Figure 2-9(b), the ionic flux of  $\text{OH}^-$  is significant when pH exceeds ca. 10, and it becomes the largest among that of other



species when pH exceeds ca. pH 11. As  $|V|$  is raised from 0.3 V to 1 V,  $S$  decreases. This is because a strong  $V$  yields a strong electric osmotic flow (EOF) so that the ionic distribution established by EDL overlapping driving cations flow is disturbed. This phenomenon is pronounced when  $C_b$  is low and/or  $V < 0$ . This is because if  $C_b$  is high, the corresponding EDL is thin so that the disturbing of  $V$  on the EDL overlapping is insignificant. If  $V < 0$ , both cations and anions are enriched in the nanopore, and therefore, the disturbing of EDL overlapping by  $V$  is advantageous to the flow of anions through the nanopore. If  $V > 0$ , the anions in the nanopore are depleted so that the ionic current is mainly contributed by cations, and the increase in the flux of anions by raising  $V$  is limited. Figure 2-8 also reveals that  $S(V > 0)$  is larger than  $S(V < 0)$ , which arises from the enrichment/depletion of ions in the nanopore. We conclude that the nanopore selectivity is influenced not only by the solution pH but also by the applied potential bias. In particular, a cation-selective nanopore might become anion-selective by raising the applied potential bias.

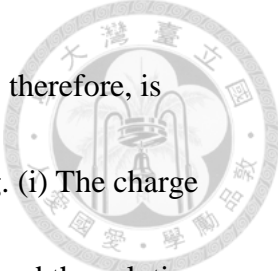
If  $\text{pH} < \text{IEP}$ , the conical nanopore is expected to be anion-selective. However, this is true only if pH is sufficiently low. Note that among the types of ion present in the liquid phase  $\text{H}^+$  has the largest mobility, and as pH decreases, its presence becomes more significant. As seen in Figure 2-9, the flux of  $\text{H}^+$  increases appreciably when pH is lower than ca. 4, and if  $C_b$  is sufficiently low (1 mM), the flux of  $\text{H}^+$  exceeds that of



anions, and therefore, dominates the selectivity  $S$ . If  $|V|$  is raised from 0.3 V to 1 V,  $S$  increases slightly, which is different from that observed for  $\text{pH} > \text{IEP}$ . As mentioned previously, a strong electric field will disturb the EDL overlapping, making it easier for co-ions to pass through. If  $\text{pH} < \text{IEP}$ , the PE layer of the nanopore is positively charged so that  $S$  increases when increasing  $|V|$ . It is interesting to note that  $S(V > 0)$  is larger than  $S(V < 0)$ . If  $V > 0$ , both cations and anions are enriched in the nanopore, and the flux of  $\text{H}^+$  increases significantly with decreasing  $\text{pH}$ . In contrast, if  $V < 0$ , both cations and anions are depleted in the nanopore, and it is uneasy for cations to pass through. Note that the flux of  $\text{H}^+$  at  $C_b = 1 \text{ mM}$  for  $V > 0$  is much larger than that for  $V < 0$ . Although ions depletion occurs when  $V < 0$ ,  $G(\text{pH} \neq \text{IEP})$  is not smaller than  $G(\text{pH} = \text{IEP})$  when the PE layer is uncharged. Figure 2-9(c) and (d) shows that the fluxes of  $\text{K}^+$  and  $\text{Cl}^-$  at  $C_b = 100 \text{ mM}$  are smaller than the corresponding fluxes at  $\text{pH} = \text{IEP}$ . However, because the flux of  $\text{H}^+$  increases with decreasing  $\text{pH}$  when  $\text{pH} < \text{IEP}$ , and the amount of increase is sufficiently large to compensate the decrease in the fluxes of  $\text{K}^+$  and  $\text{Cl}^-$ .

## 2-4. Conclusions

We modeled theoretically the ion transport behavior, the conductivity, and the selectivity of a conical nanopore surface modified by a pH-tunable polyelectrolyte (PE) layer. Extending previous studies, where constant surface charge density is usually assumed, we consider the case where the charged conditions of the nanopore surface



depend upon the level of external stimuli such as the solution pH and, therefore, is closer to reality. The results gathered can be summarized as following. (i) The charge density of the PE layer depends highly on the bulk salt concentration and the solution pH. (ii) Since the ion transport behavior in the conical nanopore is governed mainly by its surface charges, both the ion conductance and the ion selectivity vary significantly with the bulk salt concentration and the solution pH. (iii) Due to the asymmetry geometry of the conical nanopore, ion enrichment or depletion occurs in the nanopore, depending upon the direction of the applied electric field. It also depends upon the level of the bulk salt concentration. (iv) If both cations and anions are depleted (enriched) in the nanopore, the degree of depletion (enrichment) increases with increasing  $|V|$ , and  $G$  decreases (increases) and  $S$  decreases (increases), accordingly. (v) However, if pH is either sufficiently low or sufficiently high (i.e., the concentration of  $H^+$  or  $OH^-$  is comparable to the bulk salt concentration), the ion transport behavior is dominated by  $H^+$  or  $OH^-$ . For example, a positively (negatively) charged nanopore is cation (anion)-selective, and its conductivity increases with decreasing (increasing) pH when pH is sufficiently low (high). These results provide necessary information for both device design and experimental data interpretation.



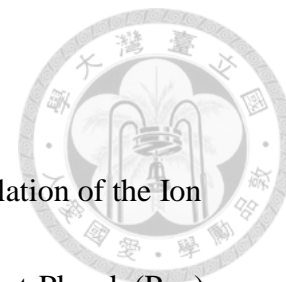


## References

1. White, H. S.; Bund, A., Ion Current Rectification at Nanopores in Glass Membranes. *Langmuir* **2008**, *24*, 2212-2218.
2. Zhang, B. K.; Ai, Y.; Liu, J.; Joo, S. W.; Qian, S. Z., Polarization Effect of a Dielectric Membrane on the Ionic Current Rectification in a Conical Nanopore. *J Phys Chem C* **2011**, *115*, 24951-24959.
3. Lin, D. H.; Lin, C. Y.; Tseng, S.; Hsu, J. P., Influence of Electroosmotic Flow on the Ionic Current Rectification in a Ph-Regulated, Conical Nanopore. *Nanoscale* **2015**, *7*, 14023-14031.
4. Lin, C. Y.; Yeh, L. H.; Hsu, J. P.; Tseng, S., Regulating Current Rectification and Nanoparticle Transport through a Salt Gradient in Bipolar Nanopores. *Small* **2015**, *11*, 4594-4602.
5. Sparreboom, W.; van den Berg, A.; Eijkel, J. C. T., Principles and Applications of Nanofluidic Transport. *Nat Nanotechnol* **2009**, *4*, 713-720.
6. He, Y.; Gillespie, D.; Boda, D.; Vlassiuk, I.; Eisenberg, R. S.; Siwy, Z. S., Tuning Transport Properties of Nanofluidic Devices with Local Charge Inversion. *J Am Chem Soc* **2009**, *131*, 5194-5202.
7. Guo, W., et al., Current Rectification in Temperature-Responsive Single Nanopores. *Chemphyschem* **2010**, *11*, 859-864.



8. Liu, J.; Kvetny, M.; Feng, J.; Wang, D.; Wu, B.; Brown, W.; Wang, G., Surface Charge Density Determination of Single Conical Nanopores Based on Normalized Ion Current Rectification. *Langmuir* **2012**, *28*, 1588-95.
9. Lan, W. J.; Holden, D. A.; White, H. S., Pressure-Dependent Ion Current Rectification in Conical-Shaped Glass Nanopores. *J Am Chem Soc* **2011**, *133*, 13300-13303.
10. Plett, T.; Shi, W. Q.; Zeng, Y. H.; Mann, W.; Vlasiouk, I.; Baker, L. A.; Siwy, Z. S., Rectification of Nanopores in Aprotic Solvents - Transport Properties of Nanopores with Surface Dipoles. *Nanoscale* **2015**, *7*, 19080-19091.
11. Pu, Q. S.; Yun, J. S.; Temkin, H.; Liu, S. R., Ion-Enrichment and Ion-Depletion Effect of Nanochannel Structures. *Nano Lett* **2004**, *4*, 1099-1103.
12. Wang, X. W.; Xue, J. M.; Wang, L.; Guo, W.; Zhang, W. M.; Wang, Y. G.; Liu, Q.; Ji, H.; Ouyang, Q. Y., How the Geometric Configuration and the Surface Charge Distribution Influence the Ionic Current Rectification in Nanopores. *J Phys D Appl Phys* **2007**, *40*, 7077-7084.
13. Kubeil, C.; Bund, A., The Role of Nanopore Geometry for the Rectification of Ionic Currents. *J Phys Chem C* **2011**, *115*, 7866-7873.
14. Cervera, J.; Ramirez, P.; Mafe, S.; Stroeve, P., Asymmetric Nanopore Rectification for Ion Pumping, Electrical Power Generation, and Information Processing



Applications. *Electrochim Acta* **2011**, *56*, 4504-4511.

15. Wang, J. T.; Zhang, M. H.; Zhai, J.; Jiang, L., Theoretical Simulation of the Ion Current Rectification (Icr) in Nano-Pores Based on the Poisson-Nernst-Planck (Pnp)

Model. *Phys Chem Chem Phys* **2014**, *16*, 23-32.

16. Daiguji, H.; Yang, P. D.; Majumdar, A., Ion Transport in Nanofluidic Channels.

*Nano Lett* **2004**, *4*, 137-142.

17. Ai, Y.; Zhang, M. K.; Joo, S. W.; Cheney, M. A.; Qian, S. Z., Effects of

Electroosmotic Flow on Ionic Current Rectification in Conical Nanopores. *J Phys Chem C* **2010**, *114*, 3883-3890.

18. Chen, G.; Das, S., Electroosmotic Transport in Polyelectrolyte-Grafted

Nanochannels with Ph-Dependent Charge Density. *J Appl Phys* **2015**, *117*.

19. Chen, K. K.; Bell, N. A. W.; Kong, J. L.; Tian, Y.; Keyser, U. F., Direction- and

Salt-Dependent Ionic Current Signatures for DNA Sensing with Asymmetric

Nanopores. *Biophys J* **2017**, *112*, 674-682.

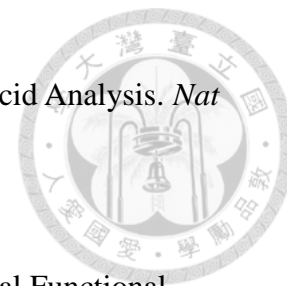
20. Sexton, L. T.; Horne, L. P.; Sherrill, S. A.; Bishop, G. W.; Baker, L. A.; Martin, C.

R., Resistive-Pulse Studies of Proteins and Protein/Antibody Complexes Using a

Conical Nanotube Sensor. *J Am Chem Soc* **2007**, *129*, 13144-13152.

21. Ai, Y.; Liu, J.; Zhang, B. K.; Qian, S., Field Effect Regulation of DNA Trans

Location through a Nanopore. *Anal Chem* **2010**, *82*, 8217-8225.



22. Venkatesan, B. M.; Bashir, R., Nanopore Sensors for Nucleic Acid Analysis. *Nat Nanotechnol* **2011**, *6*, 615-624.
23. Hou, X.; Zhang, H. C.; Jiang, L., Building Bio-Inspired Artificial Functional Nanochannels: From Symmetric to Asymmetric Modification. *Angew Chem Int Edit* **2012**, *51*, 5296-5307.
24. Ali, M.; Ramirez, P.; Mafe, S.; Neumann, R.; Ensinger, W., A Ph-Tunable Nanofluidic Diode with a Broad Range of Rectifying Properties. *Acs Nano* **2009**, *3*, 603-608.
25. Yameen, B.; Ali, M.; Neumann, R.; Ensinger, W.; Knoll, W.; Azzaroni, O., Synthetic Proton-Gated Ion Channels Via Single Solid-State Nanochannels Modified with Responsive Polymer Brushes. *Nano Lett* **2009**, *9*, 2788-2793.
26. Buchsbaum, S. F.; Nguyen, G.; Howorka, S.; Siwy, Z. S., DNA-Modified Polymer Pores Allow Ph- and Voltage-Gated Control of Channel Flux. *J Am Chem Soc* **2014**, *136*, 9902-9905.
27. Hou, X.; Guo, W.; Jiang, L., Biomimetic Smart Nanopores and Nanochannels. *Chem Soc Rev* **2011**, *40*, 2385-2401.
28. Xiao, K.; Xie, G. H.; Li, P.; Liu, Q.; Hou, G. L.; Zhang, Z.; Ma, J.; Tian, Y.; Wen, L. P.; Jiang, L., A Biomimetic Multi-Stimuli-Response Ionic Gate Using a Hydroxypyrene Derivation-Functionalized Asymmetric Single Nanochannel. *Adv Mater*



**2014**, 26, 6560-6565.

29. Liu, Q.; Xiao, K.; Wen, L. P.; Dong, Y.; Xie, G. H.; Zhang, Z.; Bo, Z. S.; Jiang, L.,

A Fluoride-Driven Ionic Gate Based on a 4-Aminophenylboronic Acid-Functionalized

Asymmetric Single Nano Channel. *Acs Nano* **2014**, 8, 12292-12299.

30. Wen, L. P.; Tian, Y.; Ma, J.; Zhai, J.; Jiang, L., Construction of Biomimetic Smart

Nanochannels with Polymer Membranes and Application in Energy Conversion

Systems. *Phys Chem Chem Phys* **2012**, 14, 4027-4042.

31. Domene, C.; Vemparala, S.; Furini, S.; Sharp, K.; Klein, M. L., The Role of

Conformation in Ion Permeation in a K<sup>+</sup> Channel. *J Am Chem Soc* **2008**, 130, 3389-

3398.

32. Garcia-Gimenez, E.; Alcaraz, A.; Aguilera, V. M., Overcharging Below the

Nanoscale: Multivalent Cations Reverse the Ion Selectivity of a Biological Channel.

*Phys Rev E* **2010**, 81.

33. Ali, M.; Schiedt, B.; Neumann, R.; Ensinger, W., Biosensing with Functionalized

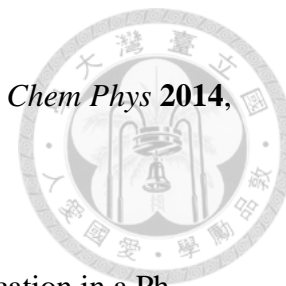
Single Asymmetric Polymer Nanochannels. *Macromol Biosci* **2010**, 10, 28-32.

34. Liu, M. Y.; Zhang, H. C.; Li, K.; Heng, L. P.; Wang, S. T.; Tian, Y.; Jiang, L., A

Bio-Inspired Potassium and Ph Responsive Double-Gated Nanochannel. *Adv Funct*

*Mater* **2015**, 25, 421-426.

35. Zeng, Z. P.; Ai, Y.; Qian, S. Z., Ph-Regulated Ionic Current Rectification in Conical



Nanopores Functionalized with Polyelectrolyte Brushes. *Phys Chem Chem Phys* **2014**, *16*, 2465-2474.

36. Lin, J. Y.; Lin, C. Y.; Hsu, J. P.; Tseng, S., Ionic Current Rectification in a Ph-Tunable Polyelectrolyte Brushes Functionalized Conical Nanopore: Effect of Salt Gradient. *Anal Chem* **2016**, *88*, 1176-1187.

37. Zeng, Z. P.; Yeh, L. H.; Zhang, M. K.; Qian, S. Z., Ion Transport and Selectivity in Biomimetic Nanopores with Ph-Tunable Zwitterionic Polyelectrolyte Brushes. *Nanoscale* **2015**, *7*, 17020-17029.

38. Dudev, T.; Lim, C., Factors Governing the Na<sup>+</sup> Vs K<sup>+</sup> Selectivity in Sodium Ion Channels. *J Am Chem Soc* **2010**, *132*, 2321-2332.

39. Vlasiouk, I.; Smirnov, S.; Siwy, Z., Ionic Selectivity of Single Nanochannels. *Nano Lett* **2008**, *8*, 1978-1985.

40. Yeh, L. H.; Hughes, C.; Zeng, Z. P.; Qian, S. Z., Tuning Ion Transport and Selectivity by a Salt Gradient in a Charged Nanopore. *Anal Chem* **2014**, *86*, 2681-2686.

41. Tagliazucchi, M.; Rabin, Y.; Szleifer, I., Ion Transport and Molecular Organization Are Coupled in Polyelectrolyte-Modified Nanopores. *J Am Chem Soc* **2011**, *133*, 17753-17763.

42. Duval, J. F. L.; Gaboriaud, F., Progress in Electrohydrodynamics of Soft Microbial Particle Interphases. *Curr Opin Colloid In* **2010**, *15*, 184-195.

43. Ma, Y.; Xue, S.; Hsu, S. C.; Yeh, L. H.; Qian, S. Z.; Tan, H. P., Programmable Ionic Conductance in a Ph-Regulated Gated Nanochannel. *Phys Chem Chem Phys* **2014**, *16*, 20138-20146.



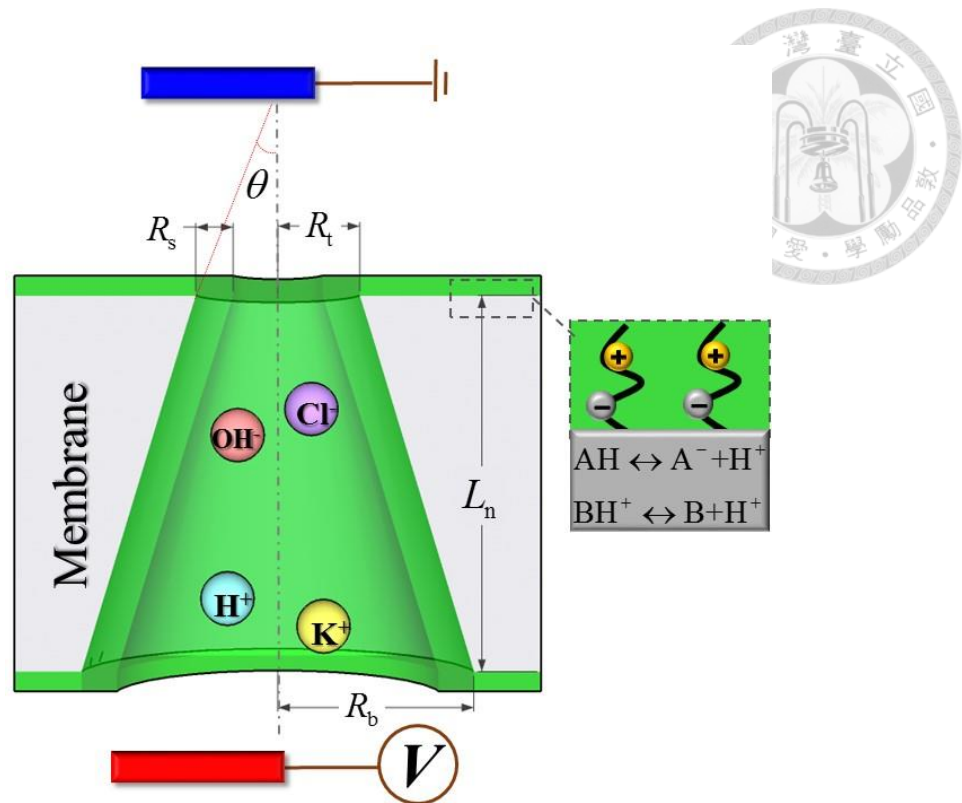


**Figure 2-1.** Schematic representation of the transport of ions in a polyelectrolyte modified conical nanopore (not to scale) subject to an applied potential bias.



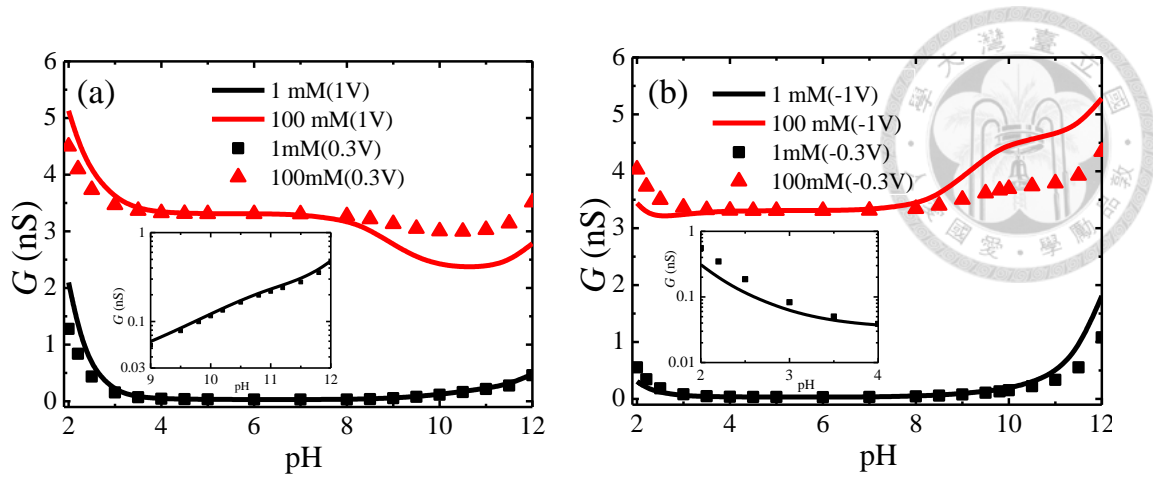


**Figure 2-2.** Variation of the nanopore conductance  $G$  with pH for positive applied potential bias, (a), and negative potential bias, (b). Curves:  $|V|=1$  V; discrete symbols:  $|V|=0.3$  V. Black curves:  $C_b=1$  mM; red curves:  $C_b=100$  mM.

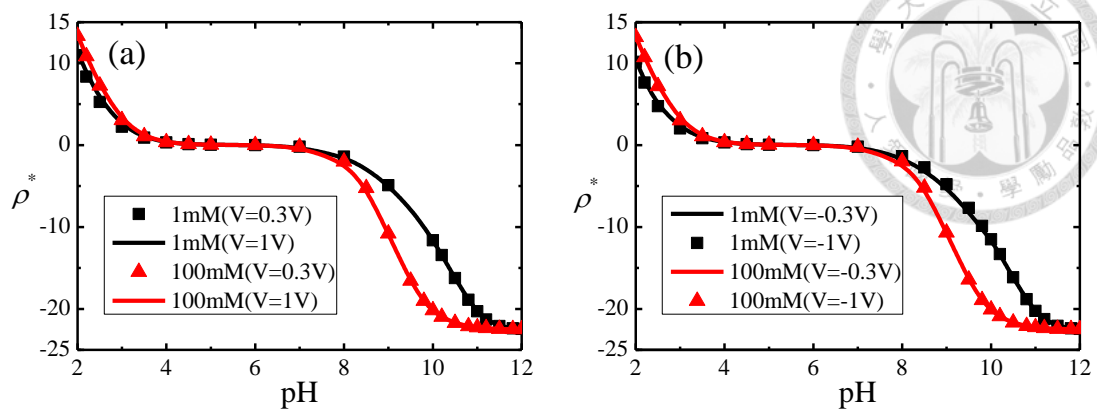


**Figure 2-3.** Variation of the volume averaged charge density of the PE layer  $\rho_a^*$  with pH for

positive, (a), and negative, (b), applied potential bias. Curves:  $|V|=1$  V; discrete symbols:

$|V|=0.3$  V. Black curves:  $C_b=1$  mM; red curves:  $C_b=100$  mM.

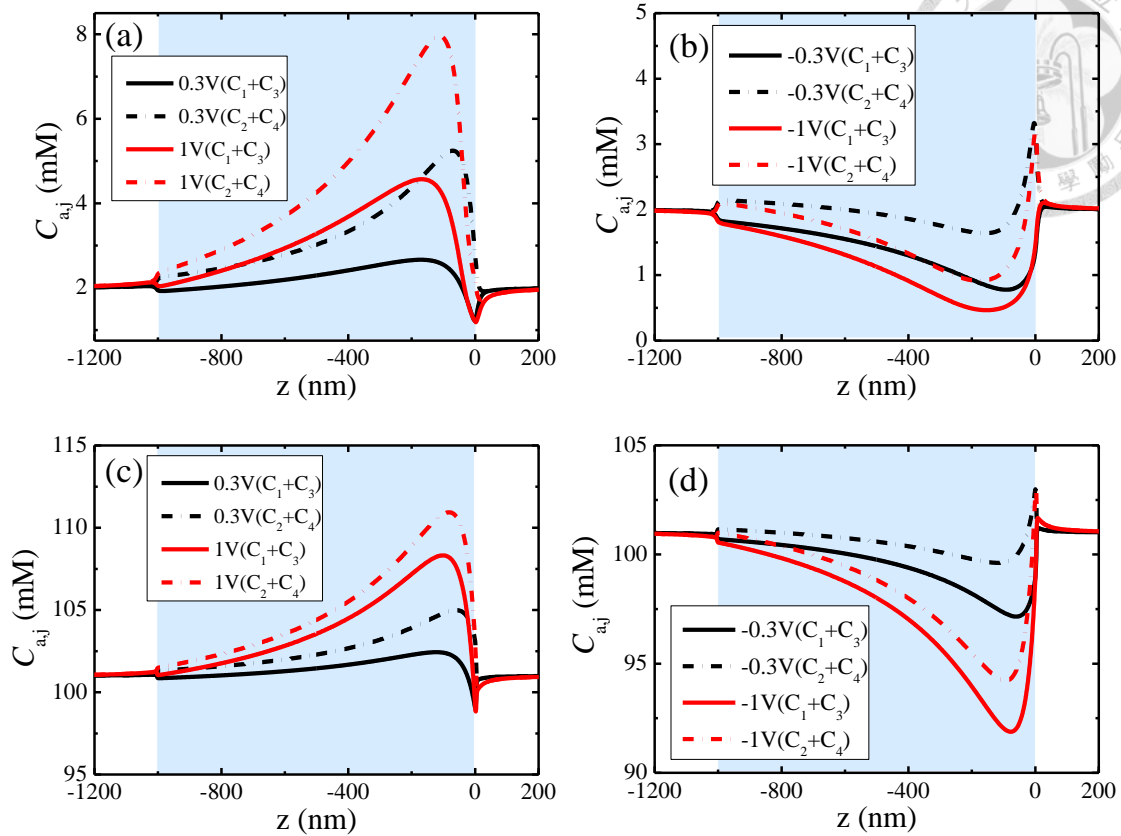


**Figure 2-4.** Axial variation in the cross-sectional averaged ionic concentrations  $C_{aj}$  at pH 3 for  $C_b=1$  mM, (a) and (b), and  $C_b=100$  mM, (c) and (d). Black curves:  $|V|=0.3$  V; red curves:  $|V|=1$  V. Solid curves: total cation concentration ( $C_1+C_3$ ); dash-dotted curves: total anion concentration ( $C_2+C_4$ ). (a) and (c):  $V>0$ ; (b) and (d):  $V<0$ .

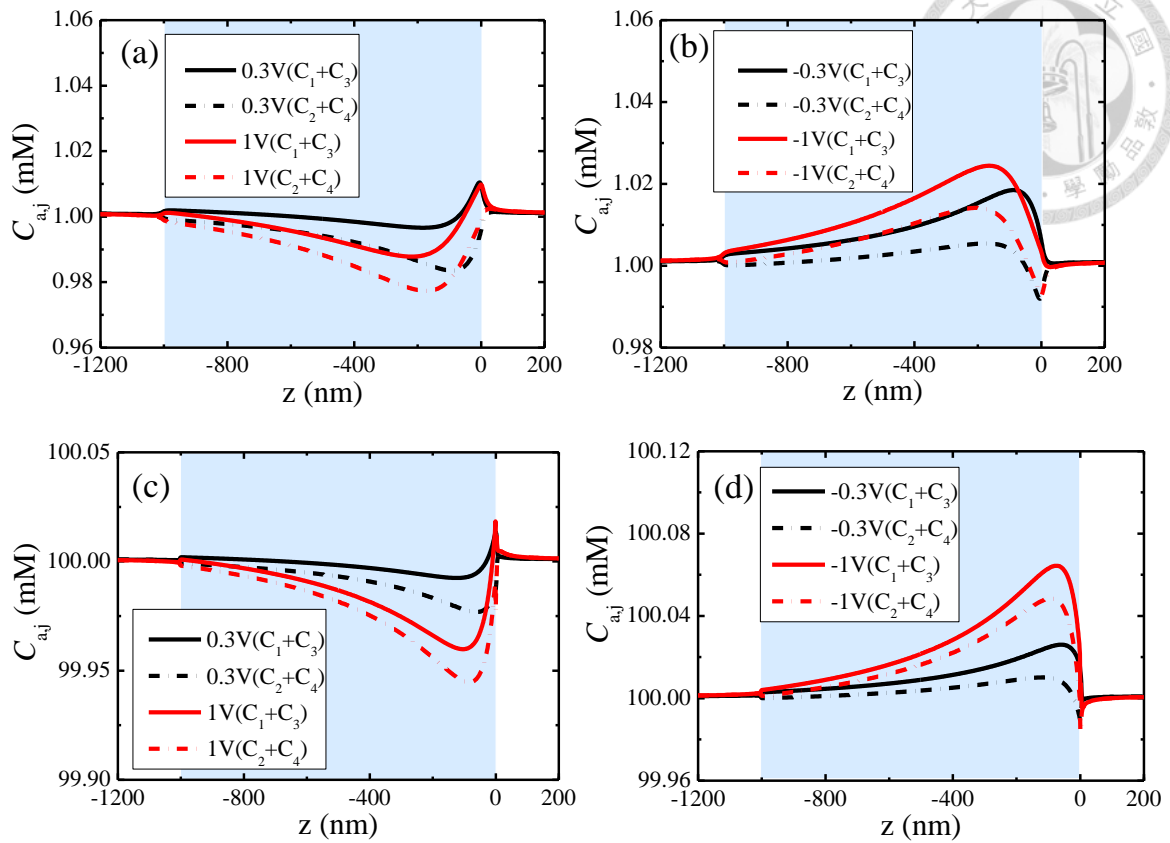


**Figure 2-5.** Axial variation in the cross-sectional averaged ionic concentrations  $C_{a,i}$  at pH 6 for  $C_b=1$  mM, (a) and (b), and  $C_b=100$  mM, (c) and (d). Black curves:  $|V|=0.3$  V; red curves:  $|V|=1$  V. Solid curves: total cation concentration ( $C_1+C_3$ ); dash-dotted curves: total anion concentration ( $C_2+C_4$ ). (a) and (c):  $V>0$ ; (b) and (d):  $V<0$ .

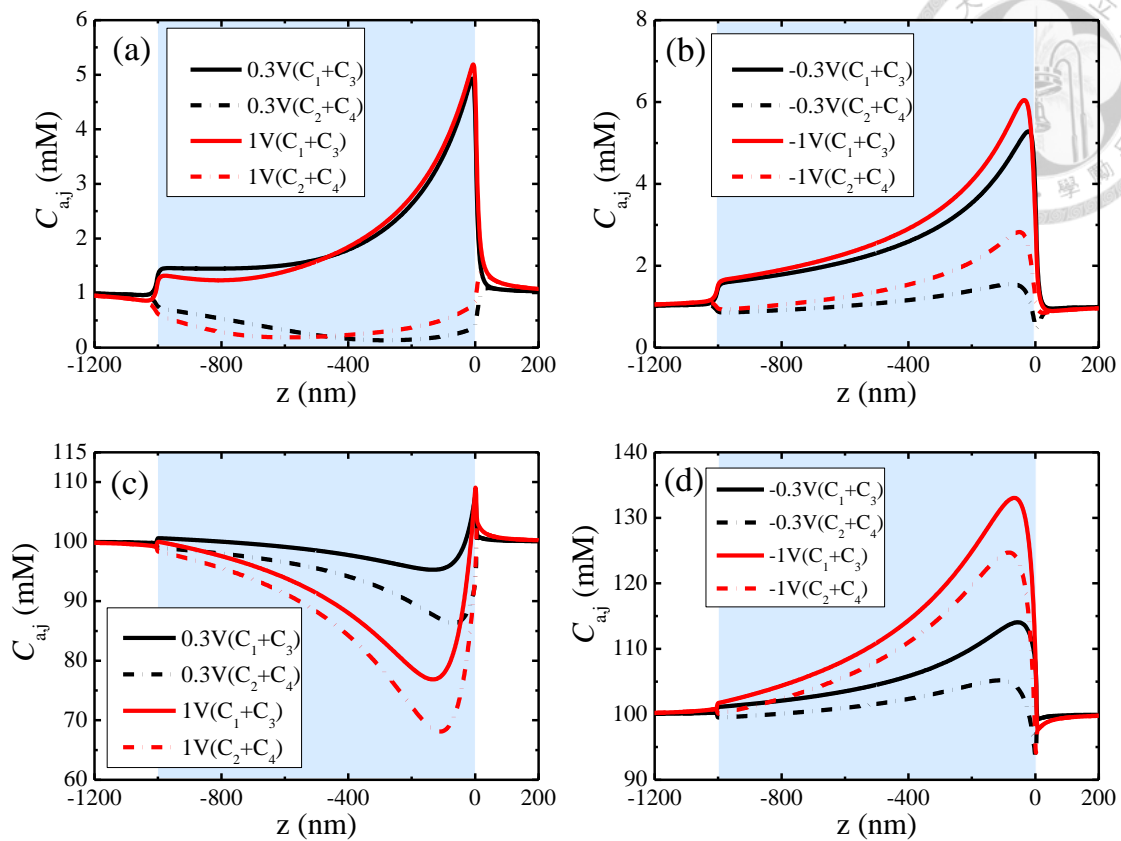


**Figure 2-6.** Axial variation in the cross-sectional averaged ionic concentrations  $C_{a,i}$  at pH 9 for  $C_b=1$  mM, (a) and (b), and  $C_b=100$  mM, (c) and (d). Black curves:  $|V|=0.3$  V; red curves:  $|V|=1$  V. Solid curves: total cation concentration ( $C_1+C_3$ ); dash-dotted curves: total anion concentration ( $C_2+C_4$ ). (a) and (c):  $V>0$ ; (b) and (d):  $V<0$ .

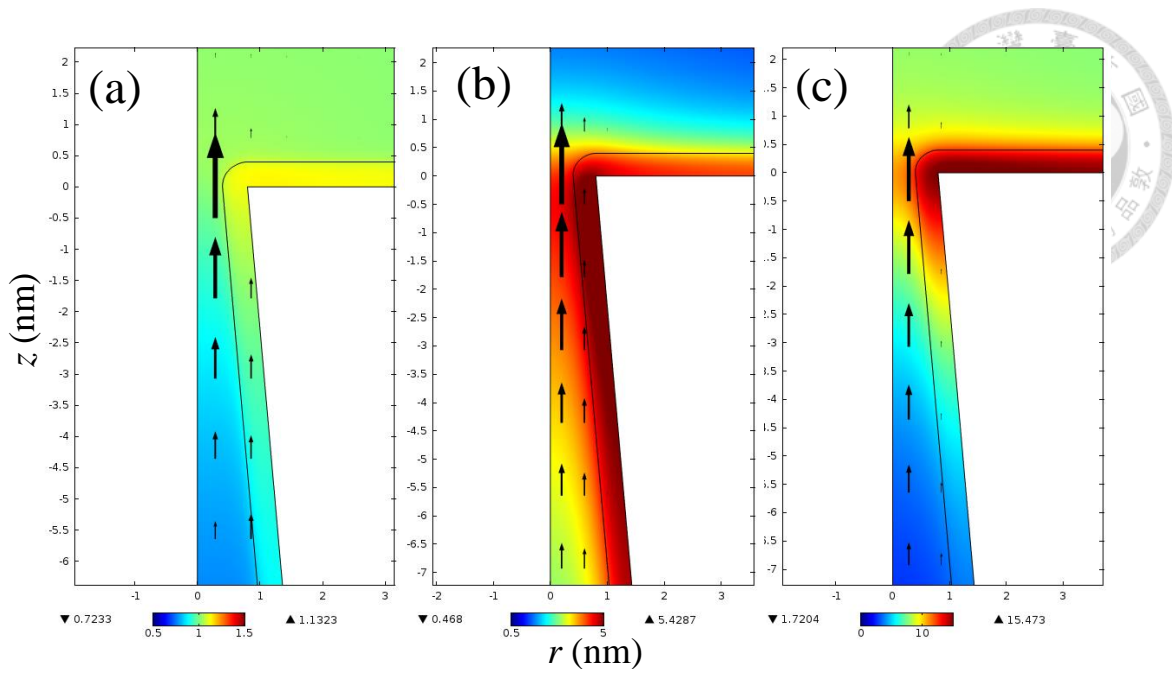


**Figure 2-7.** The fluid velocity and concentration profile near the nanopore tip for major ions. (a) and (b):  $C_1$ ; (c):  $C_2$ . (a)  $C_b=100$  mM,  $V=1$  V, and pH 9; (b)  $C_b=1$  mM,  $V=1$  V, and pH 9; (c)  $C_b=1$  mM,  $V=-1$  V, and pH 2.2. The magnitude of arrow is proportional to fluid velocity.

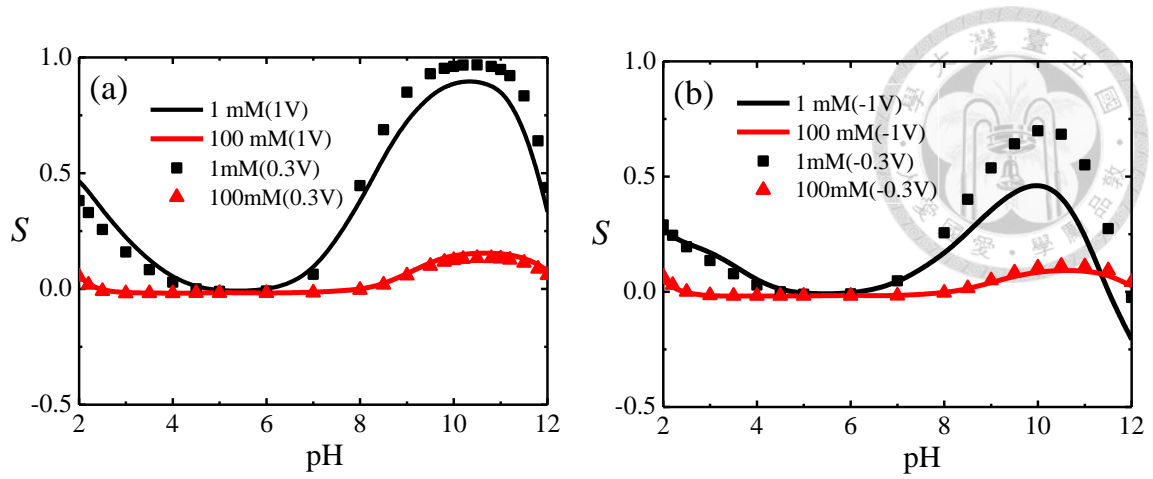


**Figure 2-8.** Variation of the nanopore selectivity  $S$  with pH for positive, (a), and negative, (b), potential bias. Curves:  $|V|=1$  V; discrete symbols:  $|V|=0.3$  V. Black curves:  $C_b=1$  mM; red curves:  $C_b=100$  mM.

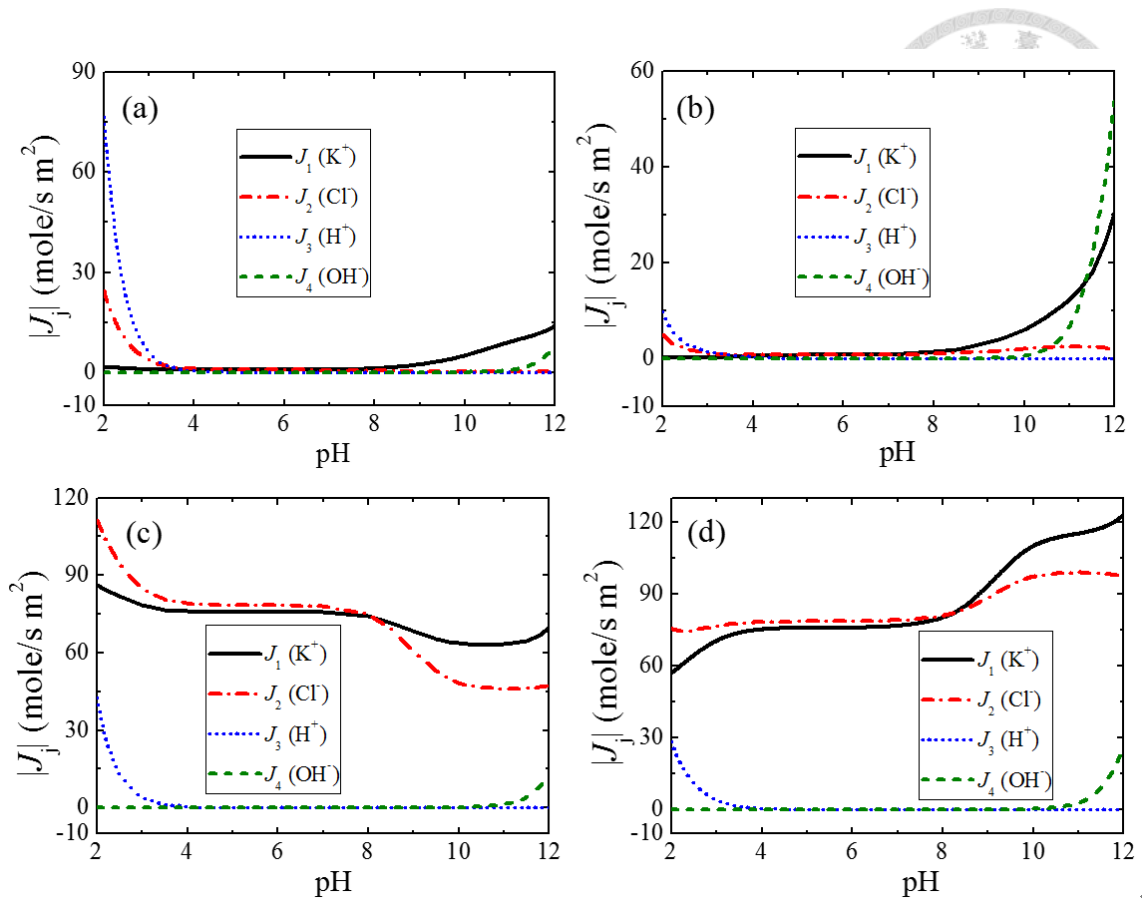


**Figure 2-9.** Variation of the cross-sectional averaged ion flux of species  $i$  at  $z=0$  with pH for  $V=+1$  V, (a) and (c), and  $V=-1$  V, (b) and (d). (a) and (b):  $C_b=1$  mM; (c) and (d):  $C_b=100$  mM.

Black solid, red dash-dotted, blue dotted, and blue dotted curves are for  $K^+$ ,  $Cl^-$ ,  $H^+$ , and  $OH^-$ , respectively.



**Table 2-1.** Values of the nanopore conductance  $G$  under various conditions.

$G$ (nS)			$V$ (V)			
			+0.3	+1	-0.3	-1
$C_b$ (mM)	1	pH 6	0.033	0.033	0.033	0.033
		pH 2	1.28	2.1	0.55	0.31
	100	pH 6	3.31	3.31	3.31	3.31
		pH 2	4.5	5.13	4.03	3.44

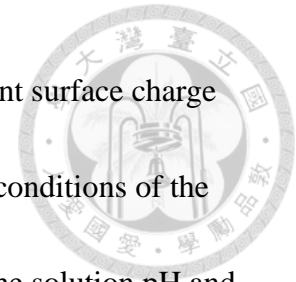


## CHAPTER 3: Conclusions



In chapter 1, the influence of electroosmotic flow (EOF) on the ionic current rectification (ICR) behavior of a conical nanopore is investigated by considering three types of aqueous salt solution, namely, LiCl, NaCl, and KCl. We show that if the EOF effect is neglected, the magnitudes of the rectification factor  $R_f$  of these solutions rank as  $\text{LiCl} > \text{NaCl} > \text{KCl}$  at each level of the applied potential bias  $V$ . However, if that effect is considered, the relative magnitudes of the  $R_f$  of the salts examined depend upon the level of  $V$ . If  $|V|$  is lower than ca. 0.9 V,  $R_f$  follows the order of  $\text{LiCl} > \text{NaCl} > \text{KCl}$ , but if  $|V|$  is higher than ca. 0.9 V, the order becomes  $\text{KCl} > \text{NaCl} > \text{LiCl}$ , which is consistent with experimental observation. At a higher  $V$ , the EOF effect is more significant, thereby influencing more appreciably the ionic concentration inside the nanopore. If  $V < 0$ , the degrees of concentration enrichment for different types of ions differ appreciably. The concentration enrichment of LiCl increases most if  $V$  is low, while that of KCl increases most if  $V$  is high, yielding the inversion of the order of  $R_f$  mentioned above. We conclude that, in addition to ionic binding, EOF also plays a crucial role in ion-species current rectification, especially when  $V$  is high.

In chapter 2, we modeled theoretically the ion transport behavior, the conductivity, and the selectivity of a conical nanopore surface modified by a pH-tunable



polyelectrolyte (PE) layer. Extending previous studies, where constant surface charge density is usually assumed, we consider the case where the charged conditions of the nanopore surface depend upon the level of external stimuli such as the solution pH and, therefore, is closer to reality. The results gathered can be summarized as following. (i) The charge density of the PE layer depends highly on the bulk salt concentration and the solution pH. (ii) Since the ion transport behavior in the conical nanopore is governed mainly by its surface charges, both the ion conductance and the ion selectivity vary significantly with the bulk salt concentration and the solution pH. (iii) Due to the asymmetry geometry of the conical nanopore, ion enrichment or depletion occurs in the nanopore, depending upon the direction of the applied electric field. It also depends upon the level of the bulk salt concentration. (iv) If both cations and anions are depleted (enriched) in the nanopore, the degree of depletion (enrichment) increases with increasing  $|V|$ , and  $G$  decreases (increases) and  $S$  decreases (increases), accordingly. (v) However, if pH is either sufficiently low or sufficiently high (i.e., the concentration of  $H^+$  or  $OH^-$  is comparable to the bulk salt concentration), the ion transport behavior is dominated by  $H^+$  or  $OH^-$ . For example, a positively (negatively) charged nanopore is cation (anion)-selective, and its conductivity increases with decreasing (increasing) pH when pH is sufficiently low (high). These results provide necessary information for both device design and experimental data interpretation.

## APPENDIX A

### Ionic Current Rectification in a Conical Nanopore: Influences of Electroosmotic Flow and Type of Salt

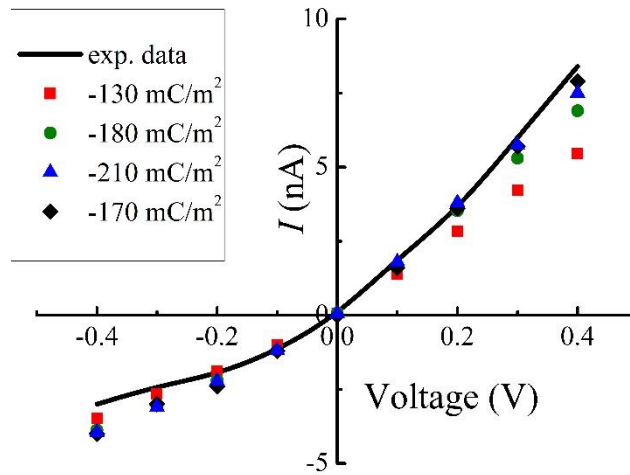
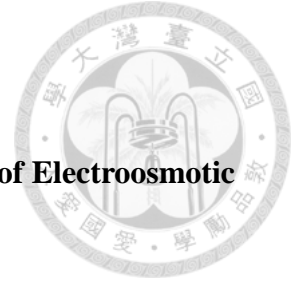


**Figure S1.** Variation of ionic current with applied electric potential bias. Solid curve: experimental data of Liu *et al.*<sup>1</sup>; discrete symbols: values predicted by the present model for various values of  $\sigma_w$  at  $L_n=10000$  nm,  $R_t=26$  nm,  $R_b=2000$  nm, and  $C_0=50$  mM.

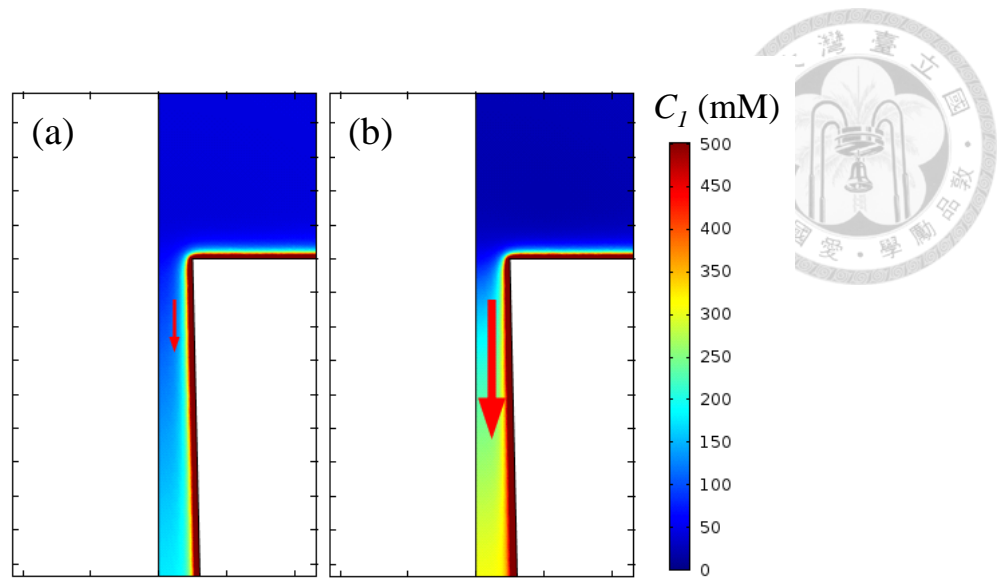


**Figure S2.** The fluid velocity and concentration profile near nanopore tip at  $V = -0.5V$ , (a), and  $V = -1.5V$ , (b). The arrow scale is proportional to fluid velocity.

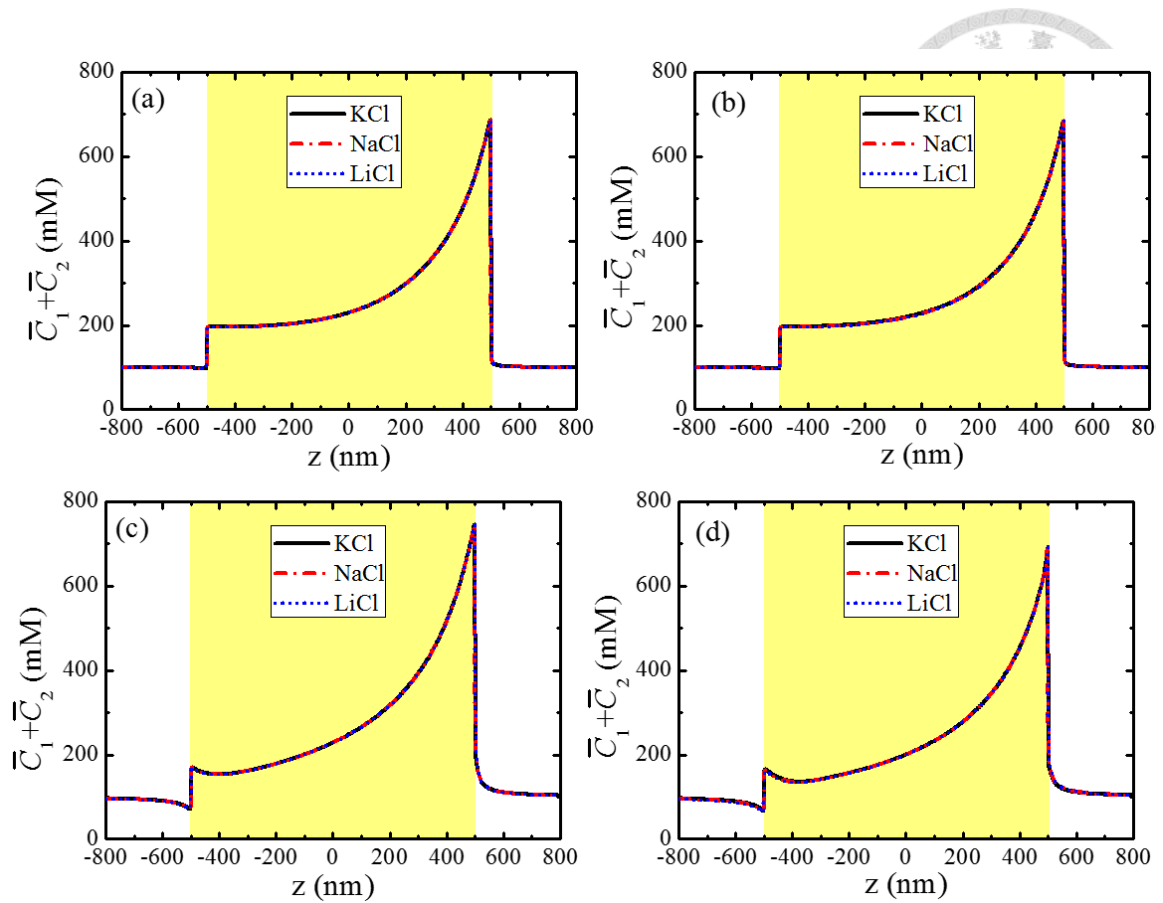


**Figure S3.** Axial variation in the cross sectional averaged concentrations under various conditions at  $C_0=50$  mM. (a) PNP model at  $V=0.2V$ , (b) (PNP+NS) model at  $V=0.2V$ , (c) PNP model at  $V=2V$ , (d) (PNP+NS) model at  $V=2V$ .

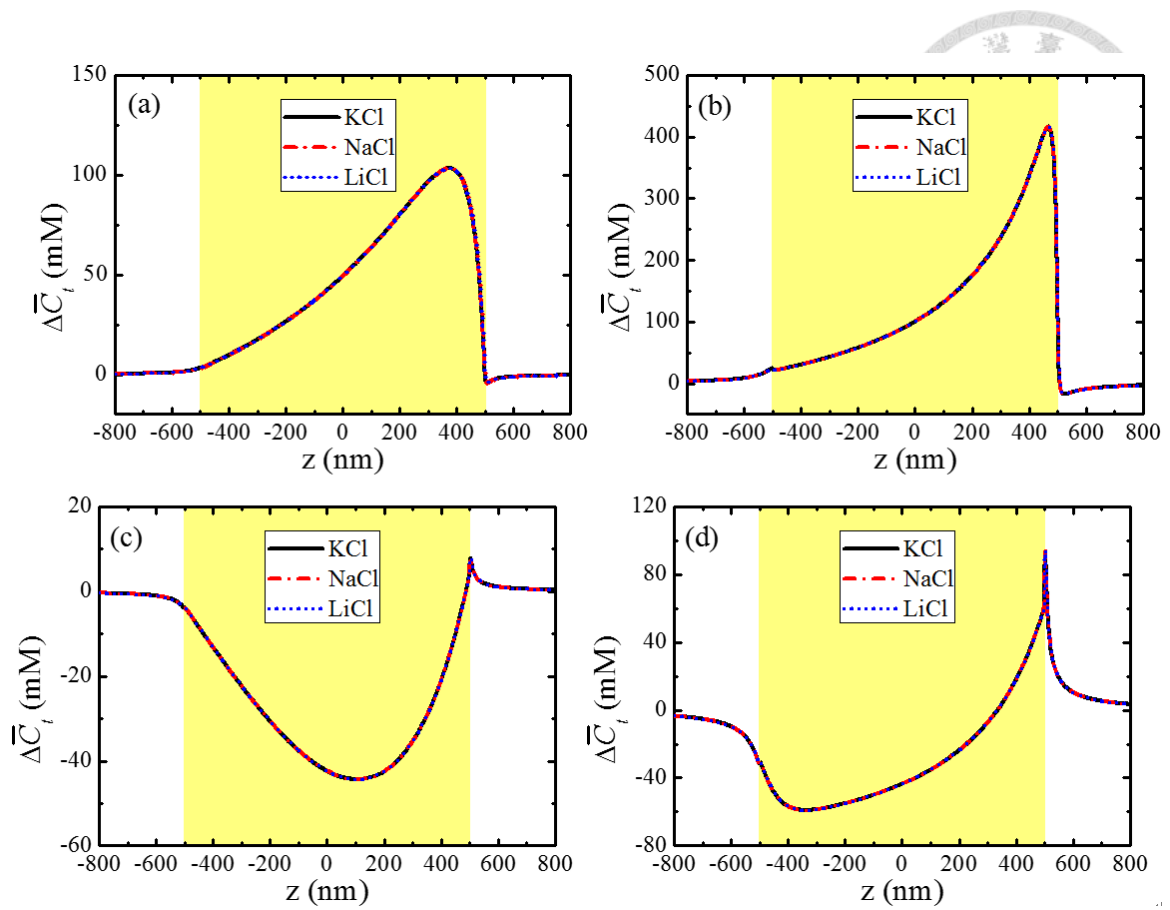


**Figure S4.** Axial variations in the cross sectional averaged concentration difference for various levels of applied bias; PNP model is applied. (a)  $V=-0.2$  V, (b)  $V=-2$  V, (c)  $V=0.2$  V, (d)  $V=2$  V.



## Reference

1. Liu, J.; Kvetny, M.; Feng, J.; Wang, D.; Wu, B.; Brown, W.; Wang, G., Surface Charge Density Determination of Single Conical Nanopores Based on Normalized Ion Current Rectification. *Langmuir* **2012**, 28, 1588-95.